TITLE

Novel therapy for gastric cancer peritoneal dissemination using genetically modified dental pulp cells and astatine-211

AUTHORS

Komei Kuge[1,2], Wan-Ying Du[1], Hiroki Masuda[1,2], Tomohiko Yasuda[1,2], Toshifumi Tatsumi[3], Xiaojie Yin[4], Masao Yoshino[5], Akira Sugiyama[6], Ryohei Numata[7], Wataru Yokoyama[7], Hidenori Shibahara[7], Tomoko Tanaka[3], Mika Kobayashi[3], Akashi Taguchi[3], Takahide Kohro[8], Naoko Takubo[3], Masahiro Nakamura[3], Jaewoong Jang[3], Yoshitaka Kumakura[3,9], Hiroshi Yoshida[2], Akira Yoshikawa[5,10], Hiromitsu Haba[4], Youichiro Wada[3]*, Kiwamu Imagawa[7]**, and Sachiyo Nomura[1,3,6]***

CORRESPONDENCE

*Co-corresponding author. Email: wada-y@ric.u-tokyo.ac.jp

** Co-corresponding author. Email: imagawa-k@jp.jcrpharm.com

*** Co-corresponding author. Email: sachiyo.nomura1012@gmail.com

AFFILIATIONS

19 [1] Department of Gastrointestinal Surgery, Graduate School of Medicine, The University of Tokyo

20 [2]Department of Surgery, Graduate School of Medicine, Nippon University

21 [3]Isotope Science Center, The University of Tokyo

22 [4]Nishina Center for Accelerator-Based Science, RIKEN

23 [5]Institute for Materials Research, Tohoku University

24 [6]Clinical Pharmaceutical Sciences, School of Pharmacy and Pharmaceutical Sciences, Hoshi

25 University

26 [7]Regenerative Medicine Unit, Drug Discovery Research Institute, Research Division, JCR

27 Pharmaceuticals Co., Ltd.

28 [8] Department of Clinical Informatics, Jichi Medical School

29 [9]Department of Diagnostic Radiology and Nuclear Medicine, Saitama Medical Center, Saitama

30 Medical University

31 [10]New Industry Creation Hatchery Center, Tohoku University

32

33 **SUMMARY**

34 Peritoneal dissemination of gastric cancer is a terminal stage with limited treatment

35 options and a five-year survival rate below 10%. To develop a more effective treatment, we

36 created a new approach that uses genetically engineered human dental pulp cells (DPCs) that

express the sodium/iodide symporter (NIS). These cells (NIS-DPCs) deliver astatine-211 (At-211) directly to tumor sites. When injected intraperitoneally into a mouse model of gastric cancer dissemination, DPCs, which were isolated and expanded, showed strong tumor-homing ability. Chemotaxis mediated by the CXCR4/SDF-1 axis has been reported to play a role in this accumulation. In addition to histological analysis, fluorescent imaging confirmed the selective accumulation of NIS-DPCs within tumor lesions. Introducing the NIS gene markedly increased SLC5A5 expression, enabling efficient At-211 uptake. To avoid nonspecific binding, sodium At-211 was utilized. High-resolution alpha-particle imaging visualized alpha-ray emission specifically from NIS-DPCs, confirming the radionuclide's intracellular retention. *In vivo*, the sequential administration of NIS-DPCs, followed by Na[At-211], resulted in the pronounced regression of peritoneal tumors and a significant extension of survival compared to controls. The therapeutic mechanism involves three coordinated steps: tumor-directed migration of NIS-DPCs, At-211 uptake via NIS transporters, and localized alpha-particle–mediated cytotoxicity. This study introduces the novel concept of cell-based alpha-radiotherapy, which integrates regenerative and nuclear medicine. Due to the well-documented safety profile of DPCs in human clinical trials (J-REPAIR, jRCT1080224505), the NIS-DPC platform emerges as a promising approach for the precise, localized irradiation of disseminated gastric cancer and other challenging malignancies.

55

56 **INTRODUCTION**

57 Peritoneal dissemination, a common terminal manifestation of gastric cancer, is
58 classified as stage IV disease. It has a 5-year survival rate of less than 10%. Current therapeutic
59 options are largely palliative, highlighting the urgent need for new treatment strategies with
60 curative potential (Ref. Kanda, 2020).

61 Previously, we established a murine gastric cancer peritoneal dissemination cell line
62 (YTN16) (Ref. Yamamoto 2018) and demonstrated the efficacy of targeted alpha-particle therapy
63 using astatine-211 (At-211) (Ref. Watabe, 2025), a radionuclide with a high linear energy transfer
64 and a 7.2-hour half-life. An anti-fibroblast growth factor receptor 4 (FGFR4) antibody, selected
65 for its high expression on YTN16 cells, was conjugated to At-211 via a halogen-tin exchange
66 reaction. *In vivo* biodistribution studies in a syngeneic C57BL/6J peritoneal dissemination model
67 revealed that intraperitoneal administration resulted in peak peritoneal radioactivity at 4.5 hours.
68 This treatment produced significant tumor regression and extended survival compared with
69 untreated controls.

70 However, the therapeutic window is limited by the time required for antigen-antibody
71 binding (approximately 24 hours) and the physical half-life of At-211. To improve delivery
72 kinetics, we sought a vehicle capable of rapidly homing to the tumor microenvironment. Tumors

73 actively recruit stromal fibroblasts to form cancer-associated fibroblasts (CAFs), and
74 mesenchymal stem cells (MSCs) have similar tumor-tropic properties (Ref. Rosu, 2024). We
75 investigated dental pulp cells (DPCs), developed by JCR Pharmaceuticals, as a potential vehicle.
76 DPCs have an established manufacturing process and have been demonstrated to be safe in a
77 phase 1/2 clinical trial for acute ischemic stroke (Ref. jRCT1080224505).

78 In this study, we evaluate NIS-DPCs as a biologic vector for targeted alpha-particle
79 therapy in gastric cancer peritoneal dissemination. We hypothesize that leveraging the tumor-
80 homing ability of NIS-DPCs can facilitate the delivery of At-211 to the tumor niche, thereby
81 overcoming the limitations of radioimmunotherapy and enabling improved therapeutic efficacy
82 and survival outcomes.

83

84

85

RESULTS

Preparation and characteristics of DPCs

Dental pulp cells (DPCs) are located in dental pulp, which is the soft connective tissue found inside teeth (Figure 1a). These cells play a key role in tooth vitality by producing dentin, supporting sensory functions, and participating in immune defense and tissue repair (Ref. Nito). Following dental pulp extraction, mild enzymatic digestion was performed to loosen the extracellular matrix. Then, mechanical mincing produced small tissue pieces. These explants were placed in culture to allow for the maintenance and expansion of DPCs (Ref. Gronthos) (Figure 1b). DPCs were able to expanded using a culture medium; however, no proliferation was observed in soft agar, suggesting that they were not tumorigenic when injected *in vivo* (Figure 1c).

Confirmation of DPC accumulation in peritoneal tumor tissue

To evaluate the specificity of tumor-directed accumulation, 1.0×10^6 DPCs were injected intraperitoneally into a previously established gastric cancer mouse model (Ref. Nagaoka). Two days after the final DPC injection, the mice were sacrificed and their peritoneal tissues were fixed and stained immunohistochemically using an anti-human Lamin B1 antibody. Brown staining, which indicates DPC localization, was observed in tissues surrounding established tumor lesions (Figures 2a and 2b), whereas no staining was detected in tissues lacking

104 tumor cell engraftment (Figure 2c). These results suggested that intraperitoneally administered
105 DPCs migrate to and accumulate within peritoneal dissemination sites.

106 To validate the migratory ability of DPCs toward the YTN16 cell line, a migration assay
107 was performed using a Transwell chamber. After 1.0×10^5 DPCs were placed in the upper
108 chamber, different numbers of YTN16 cells were placed in the lower chamber. The cells that
109 migrated to the other side of the micropore membrane were stained with a calcein solution, and
110 the absorbance was measured. Figure 2d shows that the presence of YTN16 cells induces DPC
111 migration in a cell number-dependent manner, proving the migratory capability of DPCs towards
112 YTN16 cells.

113

114 **Functional transduction of NIS to DPC**

115 The sodium-iodide symporter (NIS) is a transmembrane glycoprotein with 13
116 transmembrane domains that transports radioactive isotopes, such as I-131, I-123, I-125, I-124,
117 Tc-99m, Re-188, and At-211, into cells (see reference by Darrouzet). We introduced the NIS
118 gene (SLC5A5) into DPC cells using lentivirus. Although the expression levels of other NIS-
119 encoding genes, such as SLC26A4 and SLC26A7, remained unchanged, the expression level of
120 SLC5A5 in NIS-DPC increased by over 100-fold (Figure 3a).

121 Next, we verified the expression level of NIS molecules on the cell surface. Then, we

122 evaluated the correlation between uptake capacity and positive rate using iodine as a surrogate
123 molecule *in vitro*. The results are shown in Figures 3b and 3c. We observed that iodine uptake
124 increased in a manner dependent on the NIS-positive rate and observed a trend in which higher
125 NIS-positive rates correlated with higher iodine uptake (Figure 3b). When we measured iodine
126 uptake in three lots of NIS-DPC cells, we observed more iodine uptake was observable compared
127 to DPC cells without gene introduction. These results confirmed that the introduced NIS gene was
128 expressed on the cell surface and that its function was maintained (Figure 3c).

129 To investigate whether NIS-DPCs could preserve the ability to accumulate in tumors,
130 we first compared the localization of disseminated lesions and NIS-DPCs using fluorescent dye
131 staining. Briefly, 5.0 x 10^5 cells of NIS-DPCs were prepared as described in the Materials and
132 Methods section. Then, the cells were labeled with a fluorescent dye (DiR) for live cells, and were
133 administrated into peritoneal cavity of dissemination models. After 24 hours, the mouse models
134 were euthanized and their peritoneal surfaces were opened to apply a fluorescence detection
135 camera. The localization of the injected NIS-DPCs was visualized using an *in vivo* imaging
136 system (IVIS Lumina III) and was compared with the distribution of disseminated visible lesions.
137 As shown in Figures 3d–3g, the area occupied by the lesion was surrounded by a blue line (left
138 in Figure 3d and right in Figure 3e). Fluorescent images obtained using a fluorescent camera are
139 shown in Figures 3f (left) and 3g (right). Significant colocalization was observable on both sides,

140 suggesting the accumulation of NIS-DPCs in gastric cancer cells. To validate the ability of NIS-
141 DPCs to migrate into dissemination lesions, NIS-DPCs were injected into the peritoneal cavity in
142 a manner. Two days after injection, the peritoneal tissues were subjected to immunohistochemical
143 staining using an anti-human lamin B1 antibody. Brown staining, which indicates NIS-DPC
144 localization, was observed in tissues surrounding established tumor lesions (Figures 3h and 3i),
145 whereas no staining was detected in tissues lacking tumor cell engraftment (Figure 3j). A
146 migration assay revealed significant, cell-number-dependent migration of NIS-DPCs to YTN16
147 cells, similar to what was observed with DPCs (Figure 3k). These findings strongly suggest that
148 NIS-DPCs administered intraperitoneally accumulate within peritoneal dissemination lesions.
149

150 **Uptake of At-211 by NIS-DPC**

151 Recently, it was reported that purified At-211 undergoes nonspecific binding *in vivo*
152 due to its various chemical forms, and that this can be controlled by converting it to sodium At-
153 211 (Ref. Watabe, 2022). Therefore, prior to *in vivo* administration, we prepared sodium At -211
154 using the method shown in Figure 4a. We confirmed the uniform chemical form of the purified
155 At-211 using thin-layer chromatography (TLC) (Figure 4b).

156 Furthermore, we determined the amount of At-211 taken up by DPCs and NIS-DPCs.
157 The results are shown in Figure 4c. Similar to the results of confirming uptake capacity using a

158 surrogate molecule, NIS-DPC cells with the introduced NIS gene took up more At-211 than DPC
159 cells without the gene. Additionally, the highest uptake was observed five minutes after adding
160 At-211 when comparing changes in uptake amount over time at five, ten, and sixty minutes. These
161 results suggest that At-211 is rapidly taken up by NIS-DPC cells via the NIS protein. Therefore,
162 pre-accumulating NIS-DPC cells around the peritoneal dissemination site and then administering
163 At-211 enables the alpha-emitters to be quickly taken up by the cells and be effective within their
164 half-life.
165
166 **Novel contact scintillator imaging of alpha-ray trajectories from alpha emitters**
167 Because the NIS-DPC cell fraction was radioactive, uptake of At-211 was suggested in
168 Figure 4c. However, to verify that the alpha-rays emitted from the At-211 originate from the
169 NIS-DPC cells, a camera capable of visualizing alpha-rays on a 1-μm scale was used. Figure 5a
170 shows the alpha camera system configuration (Refs. Yamamoto, 2023; Yoshino, 2025). The
171 system comprises three principal components: (i) a 100-μm-thick GAGG thin-film scintillator
172 screen, (ii) an infinity-corrected magnification optical train consisting of an objective and an
173 imaging lens, and (iii) a CMOS imaging sensor (specifically the ORCA-Quest 2 qCMOS
174 [C15550-22UP] from Hamamatsu Photonics). Alpha-particles emitted from within the cells are
175 converted into photons by the GAGG scintillator, magnified by the 20x objective lens, and

176 detected by the CMOS sensor. Figure 5b shows an overview of the system. Eighteen thousand
177 NIS-DPC and DPC cells were cultured in an eight-well chamber slide. Then, 500 kBq of At-211
178 was added to the culture medium per well, followed by a 30-minute incubation period. The cells
179 were fixed with formalin and observed with an alpha camera for ten minutes. Figures 5c and 5f
180 show overviews of the NIS-DPC and DPC cells, respectively. Both exhibit similar morphology
181 and distribution. However, Figures 5d and 5g show that the alpha-particle range was detected
182 only in the NIS-DPC cells. Figures 5e and 5h are merged images of cells and alpha-rays.
183 Colocalization of alpha-ray and cell images was only observable in NIS-DPC cells treated with
184 At-211. These results suggest that the NIS-DPC cells efficiently took up At-211 and emitted
185 alpha-rays.
186
187 **At-211 and NIS-DPC cell administration showed antitumor effects**
188 Then, we evaluated the antitumor effects and survival prolongation associated with the
189 combined administration of NIS-DPCs and At-211 using a mouse peritoneal dissemination model.
190 Two weeks after tumor cell transplantation, we administered 0.6 MBq of At-211 per animal.
191 Twenty-four hours prior to the At-211 injection, 0.5×10^6 NIS-DPC cells were administered
192 intraperitoneally. One and a half weeks after transplantation, examination of the peritoneum
193 revealed tumor cells in the peritoneal dissemination group (Figure 6a), the NIS-DPCs

194 administration group (Figure 6b), and the DPCs and At-211 administration group (Figure 6c).
195 However, disappearance of peritoneal seeding was observed in the group that received both NIS-
196 DPCs and At-211 (Figure 6d, asterisks).

197 We evaluated the effect of NIS-DPC & At-211 treatment by scoring the antitumor
198 effects visually on a 5-point scale (0–4). This scoring was based on the extent of cancer cells
199 adhering to the peritoneal tissue at the time of death or at the end of the observation period
200 (Figure 6e).

201 Using the same evaluation scale, we performed a series of experiments to optimize the
202 At-211 radioactivity, NIS-DPC dose, and NIS-DPC injection repetition (data not shown). Based
203 on macroscopic evaluation of the extent of peritoneal dissemination, a significantly higher score
204 was achieved with 0.6 MBq of At-211/body, $5x10^5$/body of NIS-DPCs, and three
205 administrations of NIS-DPCs (data not shown).

206 The results of the antitumor effect of the optimized procedure are analyzed using
207 Turkey test and are shown in Figure 6f as a box-and-whisker plot. Compared to the untreated
208 group (no treatment) and the At-211 monotherapy group (At-211), a significant reduction in
209 score (i.e., reduction in disseminated tissue) was observed in the NIS-DPCx3+At-211 group
210 (NIS-DPCx3+At-211). Therefore, it was suggested that the administered NIS-DPC accumulated

211 around the implanted cancer cells in the peritoneum. Subsequently, the cancer tissue was

212 reduced by the cytolytic effect of alpha-rays after uptake of the administered At-211.

213 We evaluated the survival rates using this optimized regimen with Kaplan-Meier

214 curves and Logrank tests. The survival rates of individual mice in each group were evaluated

215 after At-211 administration. The results are shown in Figure 6g. Compared to the untreated and

216 At-211-treated groups, the NIS-DPCx3+At-211 group showed significantly longer survival.

217 These results suggest that the extension of the survival rate is due to the reduction and damage

218 of the implanted tumors by NIS-DPCx3+At-211 in the mouse peritoneal dissemination model.

219

DISCUSSION

In this study, we created NIS-DPC cells by forcing the expression of the NIS gene—which encodes an iodine transporter—in DPC cells that accumulate in the peritoneal cavity. Forty-eight hours after administering the cells, we introduced At-211 into the peritoneal cavity. This demonstrated that the NIS-DPC cells accumulated around the tumor cells rapidly took up At-211, resulting in tumor cell death. Figure 7 illustrates this three-step treatment method: addition of NIS-DPC cells, addition of At-211, and alpha-ray irradiation. The first step involves accumulating NIS-DPC cells in tumors. The second process involves At-211 uptake by NIS-DPC cells. The third process involves tumor-killing effects.

Accumulation of DPCs/NIS-DPCs to cancer cells

It is well-known that cancer cells accumulate large numbers of cancer-associated fibroblasts (CAFs) in their vicinity (Ref. Sahai, 2020). Furthermore, mesenchymal stem cells (MSCs) exhibit dynamics similar to those of CAFs (Ref. Antoon, 2024). MSCs migrate in response to chemokines produced by cancer cells, such as SDF-1 (Ref. Stoicov, 2013). MSCs recognize these chemokines via CXCR4. Due to protein cross-reactivity between humans and mice, however, human MSCs can also migrate toward mouse tumors. Additionally, MSCs have low immunogenicity and can be administered allogeneically. Since 2008, when it was reported

238 that DPC cells (a type of MSC) express CXCR4 and migrate in response to SDF-1 (Ref. Jiang,
239 2008), numerous studies have reported that DPC cells accumulate in inflammatory or ischemic
240 sites, particularly in oral and maxillofacial surgery (Refs. Yamaguchi, 2015; Li, 2017; Neves,
241 2020; Kornsuthisopon, 2022; Irfan, 2023). DPCs produced by JCR Pharmaceuticals have been
242 administered to humans and proven safe (Ref. Suda, 2022). They were examined for their ability
243 to migrate and accumulate around tumor tissues in a mouse peritoneal dissemination model (Ref.
244 Nagaoka, 2025).

245 As mentioned above, the first step in this therapy is the accumulation of NIS-DPC cells
246 in cancer cells. Multimodal experiments were performed to prove this. Macroscopically, as shown
247 in Figures 3d to 3g, the localization of the fluorescently labeled NIS-DPC cells coincided with
248 the localization of the gastric cancer peritoneal dissemination lesions. Microscopically, Figures
249 2a-2c and 3h-3j show that both DPCs and NIS-DPCs were present in gastric cancer lesions via
250 immunohistochemical staining. These findings suggest that DPC/NIS-DPC cells accumulate in
251 tumor cells.

252 *In vitro*, DPC/NIS-DPC cells were observed migrating toward gastric cancer cells (see
253 Figures 2d and 3k). The molecular mechanism underlying this migration is thought to involve the
254 induction of EGR1 in DPC/NIS-DPC cells by soluble factors released from the cancer cells (Ref.
255 Xiao, 2021). Further clarification of this mechanism is needed in future studies.

256

257 **Functional uptake of At-211 by NIS-DPC**

258 The second step of this treatment method involves NIS-DPC cells taking up At-211.
259 Several experiments were conducted to determine whether the introduced iodine transporter
260 functions in DPC cells. First, non-radioactive iodine and a non-radioactive ligand were added to
261 DPC cells expressing NIS, and the uptake efficiency was examined. As shown in Figures 3, the
262 amount of uptake increased in a NIS expression-dependent manner, demonstrating that NIS
263 functionally takes up the ligand (Figure 3b), and NIS-DPCs exhibited approximately 50-fold
264 higher iodine uptake than DPCs (Figure 3c). Furthermore, Figure 4c shows the efficient uptake
265 of At-211 by NIS-DPCs beginning five minutes after At-211 administration. Using the newly
266 developed alpha camera, we confirmed consistent uptake of At-211 and cell localization (Figure
267 5). This indicates that NIS-DPC cells take At-211 into the cell and emit alpha rays. In the future,
268 we expect to directly visualize the lethal effect of alpha-rays on tumor cells by co-culturing NIS-
269 DPC cells with tumor cells and observing them using the alpha camera.

270

271 **Tumoricidal effect of NIS-DPC&At-211**

272 As shown in Figure 6, this study demonstrated that administering At-211 after
273 three times NIS-DPC administration reduced peritoneal dissemination lesions and improved

survival rate. This confirms the tumor-killing effect, the third process of this treatment. When evaluating the efficacy of anticancer drugs in humans, the primary endpoint is an extension of the survival period. Therefore, improvement in survival rate is equally important when evaluating the efficacy of cancer treatments using model animals as it is in humans. Furthermore, the proposed mechanism of action was strongly implicated. However, it has been reported that the immune response induced by neoantigens released from tumor cells damaged by radiation exposure contributes to the efficacy of nuclear medicine therapy (Ref. Nagaoka, 2025). Elucidating the mechanism in greater detail in the future may expand the application of combined therapy with NIS-DPC cells and At-211.

Requirement for practical application

In order to commercialize this treatment method in the future, data on its efficacy must first be accumulated. Additionally, data on the safety and pharmacokinetics of the reagents used in this study will be necessary. Since DPC cells have previously been administered to humans and their safety has been demonstrated (Suda, 2022), data on the safety of NIS-DPCs is essential. In particular, since lentiviruses are used to introduce the NIS gene, it is necessary to determine if the viruses are excreted by the treated animals. Furthermore, since At-211 is administered as sodium astatine into the abdominal cavity, pharmacokinetic data must be obtained from medium-sized

292 animals before human administration. Human clinical studies will be conducted based on these
293 data.
294 DPC cells can be administered allogenically. Furthermore, they can be procured
295 minimally invasively, and the cells can be stored frozen, making it feasible to establish a supply
296 system. Meeting clinical demand for At-211 will be possible through the future widespread
297 adoption of mass production technology and the development of dedicated accelerators.
298
299 **Perspective**
300 Here, we reported a new treatment method combining nuclear and regenerative
301 medicine products. Since the safety of DPC cells has already been proven in humans, a first-in-
302 human trial should be conducted after the safety of NIS-DPCs and At-211 is evaluated.
303
304
305
306
307

308 **MATERIALS AND METHODS**

309 **Preparation of Dental Pulp Cells (DPCs)**

310 Human dental pulp cells (DPCs) were isolated from extracted teeth under sterile
311 conditions, as previously described with minor modifications. Briefly, extracted teeth were first
312 disinfected by immersion in 1% chlorhexidine gluconate solution followed by washing with
313 sterile physiological saline to remove debris and surface contaminants.

314 The tooth structure was mechanically fractured using a dental rongeur, and the pulp
315 tissue was carefully extracted from the pulp chamber. The obtained pulp tissue was minced into
316 small fragments using sterile surgical scissors and transferred into a tube containing Liberase
317 digestion solution (Roche Diagnostics, Basel, Switzerland). The tissue suspension was incubated
318 at 37°C for enzymatic digestion with gentle agitation until the connective matrix was adequately
319 loosened.

320 After digestion, the suspension was mixed with Dulbecco's Modified Eagle Medium
321 (DMEM) supplemented with 20% fetal bovine serum (FBS) and 1% penicillin/streptomycin (P/S)
322 to terminate the enzymatic reaction. The mixture was centrifuged at 300 × *g* for 5 minutes, and
323 the supernatant was discarded. The resulting pellet was resuspended in fresh DMEM containing
324 20% FBS and 1% P/S and seeded onto tissue culture plates.

325 Cells were incubated at 37°C in a humidified 5% CO_2 atmosphere and expanded until

326 passage 5 (P5). From passage 1 (P1) onward, cultures were maintained in DMEM supplemented
327 with 10% FBS but without antibiotics, to avoid potential effects of antimicrobial agents on cell
328 proliferation or differentiation. All procedures were conducted under aseptic conditions using
329 biosafety level 2 (BSL-2) practices.
330
331 **Soft Agar Colony Formation Assay**
332 To evaluate anchorage-independent growth and confirm the non-transformed
333 characteristics of the cells, a soft agar colony formation assay was performed using the
334 CytoSelect™ 96-Well Cell Transformation Assay Kit (Cell Biolabs, Inc., San Diego, CA, USA),
335 according to the manufacturer's protocol.
336 HeLa, DPC, and NIS-DPC cells were cultured under standard conditions until reaching
337 logarithmic growth phase. Cells were then harvested and resuspended in assay medium at the
338 following densities: 8×10^3 cells/well for HeLa, and 8×10^4 cells/well for DPC and NIS-DPC.
339 Cell suspensions were seeded in duplicate 96-well soft agar plates (Plate ① and Plate ②) as
340 described in the kit instructions.
341 Plate ① was incubated for 7 days at 37°C in a humidified 5% CO_2 incubator to allow
342 potential colony formation. Plate ② was processed immediately after cell seeding for background
343 measurement following the manufacturer's procedures: agar dissolution, cell lysis, and nuclear

344 staining. The absorbance of each well was measured using a microplate reader to determine
345 baseline optical density (OD).
346 After the 7-day incubation period, Plate ① was subjected to the same lysis and staining
347 procedures, and absorbance was measured again. Colony formation was quantified by comparing
348 OD values between the 0-day (Plate ②) and 7-day (Plate ①) samples. As expected, a significant
349 increase in OD was observed only in the HeLa group, while DPC and NIS-DPC cells showed no
350 increase, confirming their non-transformed phenotype.
351
352 **Construction of Lentiviral Vector pLVSIN-EF1α-hNIS-Pur**
353 A self-inactivating (SIN) lentiviral expression vector, pLVSIN-EF1α-hNIS-Pur, was
354 constructed based on the parental plasmid pLVSIN-EF1α-Pur (Takara Bio Inc.). The human
355 sodium/iodide symporter (hNIS) gene (sequence ID No. 2; NCBI accession number
356 NM_000453.3) was inserted into the multiple cloning site of the parental vector.
357 The DNA fragment encoding hNIS was synthesized with a Not I site at the 5′ end and a BamH I
358 site at the 3′ end. Both the hNIS insert and the pLVSIN-EF1α-Pur vector were digested with the
359 respective restriction enzymes Not I and BamH I (New England Biolabs or equivalent) to
360 generate compatible cohesive ends. The digested fragments were ligated using Ligation High
361 Ver. 2 (TOYOBO Co., Ltd.), yielding the recombinant plasmid pLVSIN-EF1α-hNIS-Pur.

362 All recombinant DNA manipulations were carried out under standard molecular cloning

363 conditions in accordance with institutional biosafety regulations.

364

365 **Lentiviral Packaging and Production**

366 Lentiviral particles carrying the pLVSIN-EF1α-hNIS-Pur construct were produced

367 using a self-inactivating lentiviral packaging system. In addition to the expression vector

368 described above, a mixture of packaging plasmids encoding HIV-1–derived structural and

369 regulatory proteins (Gag, Pol, Tat, and Rev) and the vesicular stomatitis virus G glycoprotein

370 (VSV-G) envelope was provided by the Lentiviral High Titer Packaging Mix (Takara Bio Inc.).

371 Viral particles were generated following a modified standard protocol.

372 Poly-L-lysine–coated culture dishes were seeded with cells at a density of

373 approximately 5×10^4 cells/cm² and incubated overnight at 37°C in a humidified 5% CO_2

374 incubator. On the following day, a DNA mixture was prepared by adding 7 μL of Packaging Mix

375 and 11 μL of pLVSIN-EF1α-hNIS-Pur plasmid DNA (0.5 μg/μL) to 1.5 mL of Opti-MEM I

376 Reduced Serum Medium (Gibco).

377 Transfection was performed using either FuGENE HD (Promega) or TransIT-Lenti

378 Transfection Reagent (Takara Bio Inc.), according to the manufacturers' instructions. The

379 transfected cells were incubated at 37°C in 5% CO_2 for approximately 24 hours, after which the

380 culture supernatant was replaced with 10 mL of DMEM (Gibco) and incubation continued for
381 another 24 hours.

382 The culture supernatant containing lentiviral particles was collected and clarified by
383 centrifugation at 500 × *g* for 10 minutes. The supernatant was then passed through a 0.45 μm filter
384 (Millipore, Cat. No. SLHPR33RB) to remove cellular debris. The filtered viral solution was
385 aliquoted into microtubes and stored at −80°C until use.

386

387 **Generation of hNIS-Expressing Dental Pulp Cells (hNIS-DPCs)**

388 DPCs were seeded at a density of 2.0×10^4 cells/cm² and cultured overnight at 37°C in
389 a humidified 5% CO_2 incubator. On the following day, cells were transduced with the hNIS
390 lentiviral vector (hNIS-LV) at a multiplicity of infection (MOI) of 10. To enhance viral
391 transduction efficiency, protamine sulfate (Sigma-Aldrich, Cat. No. P4020) was added to the viral
392 inoculum at a final concentration of 100 μg/mL.

393 The viral supernatant was removed 24 hours after infection and replaced with fresh
394 DMEM (Gibco, Cat. No. 10567-014). Cells were cultured with medium changes every 2–3 days,
395 and cell morphology and confluence were monitored microscopically. When cultures reached
396 approximately 90% confluence, cells were passaged using standard trypsinization procedures.
397 For selection of transduced cells, puromycin was added to the culture medium at a final

concentration of 1 μg/mL during the first passage after viral infection. Resistant colonies were expanded under puromycin selection. Thereafter, cells were maintained in standard DMEM without selection antibiotic for one to two additional passages to establish a stable hNIS-DPC line. Established cells were cryopreserved in liquid nitrogen for long-term storage.

Cell Culture

NIS-DPC and YTN16 cells were cultured in Dulbecco's modified Eagle's medium (DMEM; Gibco, Cat. No. 10567014) under standard conditions (37°C, 5% CO_2). Cells were maintained for 3 to 4 days before use.

Cell Harvesting and Co-culture Setup

Cells were detached using 0.25% trypsin–EDTA (Gibco, Cat. No. 25200056) and resuspended in fresh DMEM. Cell concentrations were adjusted to 1×10^5 cells/mL. For co-culture experiments, cells were seeded into 24-well Transwell plates (Corning, Cat. No. 353504) equipped with cell culture inserts (Corning, Cat. No. 351152). NIS-DPC cells (1×10^5 cells) were seeded in the upper insert, and YTN16 cells (1×10^5 cells) were seeded in the lower chamber. The co-cultures were incubated for 48 hours at 37°C in a humidified incubator with 5% CO_2.

416 **Migration Assay**

417 After 48 hours of co-culture, the medium was aspirated and replaced with DMEM
418 containing 1% human serum albumin (HSA) prepared from 25% clinical-grade albumin solution
419 (Takeda Pharmaceutical Co., Ltd.). Cells were stained with Calcein (Dojindo, Cat. No. 341-
420 07901) according to the manufacturer's instructions to visualize viable cells. Fluorescence
421 intensity was quantified using a spectrophotometric plate reader, and fluorescent images were
422 captured using a fluorescence microscope under identical exposure conditions for all samples.

423

424 **Preparation of Mouse Model and Application of NIS-DPC Followed by Na[At-211]**

425 Six-week-old female C57BL/6J mice were purchased from Jackson Laboratoy Japan
426 and housed in a specific pathogen-free environment at the Animal Experiment Facility in
427 Isotope Science Center, the University of Tokyo. The animal use proposal and experimental
428 protocol were reviewed and approved by the University of Tokyo Animal Committee (ID: Med-
429 P22-084、A2024ISC003). The YTN16 cell line was maintained in Dulbecco's modified
430 Eagle's medium (DMEM, Sigma-Aldrich Merck, Tokyo, Japan) with 10% heat-inactivated fetal
431 bovine serum (FBS, BWT, France), 50 μg/mL streptomycin, 50 U/mL penicillin (Thermo
432 Fisher Scientific, Tokyo, Japan), and MITO + serum extender (Corning, NY, USA). A total of
433 1.0×10^7 YTN16 cells were suspended in 500 μL of Hanks' Balanced Salt Solution and

434 intraperitoneally injected into mice (Ref. Nagaoka, 2025). Starting the following day, 2 μg of
435 thyroxine was administered orally once daily. At 8, 10, and 12 days after YTN16 cell injection,
436 0.5×10^6 NIS-DPC cells, 0.5×10^6 DPC cells, or vehicle alone were administered
437 intraperitoneally. On day 14, Na[At-211] (0.6 MBq) dissolved in 0.5 mL of vehicle was injected
438 intraperitoneally. Nine days after the last Na[At-211] injection, the peritoneal cavity was
439 examined, or the mice were observed until death or humane sacrifice, followed by examination
440 of the peritoneal cavity.

441

442 **Cell Labeling with DiR and *In Vivo* Administration**

443 NIS-DPC cells were suspended in medium at a concentration of 1×10^7 cells/mL. The
444 cell suspension was mixed with an equal volume of 20 μmol/L DiR dye solution (Thermo
445 Fisher Scientific or equivalent), resulting in a final dye concentration of 10 μmol/L. The mixture
446 was incubated for 15 minutes at room temperature in the dark, with gentle tapping every 5
447 minutes to ensure homogeneous labeling. After incubation, the cells were washed three times
448 with injection medium by centrifugation to remove excess dye. The labeled cells were
449 resuspended in injection medium at a final concentration of 1×10^6 cells/mL. Labeled NIS-DPC
450 cells were administered intraperitoneally to peritoneal dissemination model mice. All animal

experiments were conducted in accordance with institutional guidelines and approved by the relevant Animal Care and Use Committee.

In Vivo Fluorescence Imaging

At predetermined time points after injection, mice were sacrificed, and peritoneal tissues were harvested. DiR fluorescence signals were detected using an *in vivo* imaging system (IVIS Lumina III; PerkinElmer) under the following parameters: excitation filter, 740 nm; emission filter, 790 nm; and exposure time, automatic setting. Fluorescence images were analyzed using the manufacturer's software.

Production of At-211

According to the procedure described in Refs. (Yin, 2023, Yin, 2024), the radioisotope of At-211 was produced in the nuclear reaction of ^{209}Bi(α,2n)^{211}At using the AVF cyclotron of the RIKEN RI Beam Factory.

Preparation of Na[At-211]

467 Dry solid At-211 of multiple chemical species in glass vial was dissolved the injection
468 water (100 μL). At-211 aqueous solution (63 MBq, 50 μL) was mixed with 1% ascorbic acid,
469 2.3% MEYLON Injection aqueous solution (1 mL). After stirreing briefly, the reaction solution
470 of At-211 was left to stand for 1hour at room temperature under sealed condition to afford the
471 Na[At-211]. The Na[At-211] solution was dissolved 1% ascorbic acid, 2.3% MEYLON Injection
472 aqueous solution, and used animal experiments and the cell tracer experiments.
473
474 **Thin-Layer Chromatography (TLC) Analysis**
475 Thin-layer chromatography (TLC) was performed using silica gel 60 plates (Merck) as
476 the stationary phase. Samples (5 μL, 280 kBq) were spotted onto the plate and developed in a
477 solvent system consisting of acetonitrile and Milli-Q water (CH_3CN:MQ = 2:1, v/v).
478 After development, the chromatograms were analyzed using a TLC scanner (Scan-RAM;
479 LabLogic Systems Ltd.) equipped with a ZnS scintillation detector. Radioactivity on the TLC
480 plates was quantified using the manufacturer's analysis software.
481
482 **Quantitative Measurement of At-211 Uptake**
483 Na[At-211] (10 kBq) was added to the DPC and NIS-DPC cell and incubated for 5
484 minutes, 30 minutes, and 1 hour, respectively. After incubation, the medium was removed and the

485 cells were collected. The radioactivity of the samples was then measured with a gamma-counter,

486 and the counts per minute (CPM) were calculated.

487

488 **Visualization of alpha-ray**

489 Alpha-particle track images were acquired with a CMOS sensor at 1-second exposure,

490 yielding 600 frames each for NIS-DPS and DPC cells. Image analysis was conducted in ImageJ

491 (v1.54f). For each frame, a fixed intensity threshold was applied, followed by morphological

492 operations to generate a binarized mask of suprathreshold regions. Each image was then

493 accumulated with its corresponding mask to isolate regions of interest surrounding the alpha-

494 particle tracks, and the resulting stacks were Z-projected to produce composite track images.

495

ACKNOWLEDGEMENTS

The radioisotope of At-211 was produced at the RI Beam Factory operated by the RIKEN Nishina Center and the CNS, University of Tokyo, Japan. The authors gratefully acknowledge Yousuke Kanayama, Nozomi Sato, Akihiro Nambu, Tomohiro Tomitsuka, Hiromichi Shimizu, Yudai Shigekawa, Sayantani Mitra, and Keiko Watanabe of RIKEN Nishina Center for technical assistance with the At-211 production.

FUNDING

This work was supported by Grants-in-Aid for Scientific Research (KAKENHI) from the Japan Society for the Promotion of Science (JSPS), including "Basic study on internal radiotherapy utilizing stem cells" (grant number 15K06868); “Development of novel radiopharmaceuticals using α-emitting radionuclides and antibody drug delivery systems” (grant number 23H00419); “Collaborative research on therapeutic radionuclide production and radiopharmaceutical synthesis” (grant number 20KK0174); “Development of novel therapy for peritoneal dissemination using neoantigen activation induced by short-lived α-emitting radionuclides” (grant number 24K02393); “Experimental study of intraperitoneal radiotherapy for gastric cancer dissemination using highly selective short-lived alpha-particle delivery” (grant number 19H03510); and “Development of radiation imaging technology for detecting micro–peritoneal

514 dissemination of gastric cancer" (grant number 21H00169).

515 Additional support was provided by the Uehara Memorial Foundation ("Development of

516 radionuclide production technology and novel radiopharmaceuticals through accelerator

517 science") and the Nakatani Foundation for Advancement of Measuring Technologies in

518 Biomedical Engineering ("Development of theranostic technology using α-emitting

519 radionuclides").

520

521 **AUTHOR CONTRIBUTIONS**

522 S.N. conceived and supervised the study and performed animal experiments. K.K., H.Y., H.M.,

523 T.Y., and W.-Y.D. conducted animal experiments. Y.W. performed alpha-particle therapy

524 experiments and contributed to manuscript preparation. T.T. performed sodium At-211 synthesis.

525 M.K. conducted cell culture experiments. A.T. performed RNA-seq data acquisition. T.Ta.

526 analyzed pathological specimens. J.J. conducted At-211 compound analyses. Y.K. performed

527 imaging studies. A.S. carried out alpha-particle uptake assays. R.N. prepared DPC cells and

528 performed genetic modification of DPCs. W.Y. and H.S. performed functional analyses of DPCs

529 and NIS-DPCs. K.I. managed DPC manufacturing and quality control. H.H. and X.Y. developed

530 At-211 production technology. M.Yo. performed direct alpha-particle imaging. A.Yo. developed

531 scintillators. T.K. and N.T. performed bioinformatics analyses. M.N. supervised bioinformatics

and data integration. All authors discussed the results and approved the final manuscript.

COMPETING INTERESTS

N/A

DATA AND MATERIALS AVAILABILITY

under preparation

REFERENCES

A. Rosu, B. Ghaemi, J. W. M. Bulte, A. Shakeri-Zadeh. Tumor-tropic Trojan horses: Using mesenchymal stem cells as cellular nanotheranostics. ***Theranostics*** 14, 571–591 (2024). doi:10.7150/thno.90187.

A randomized, double-blind, placebo-controlled, multicenter study to evaluate the safety and efficacy of JTR-161 in patients with acute ischemic stroke (jRCT1080224505). ***Japan Registry of Clinical Trials***, registered in 2022.

C. Nito, K. Sowa, M. Nakajima, Y. Sakamoto, S. Suda, Y. Nishiyama, A. Nakamura-Takahashi, Y. Nitahara-Kasahara, M. Ueda, T. Okada, and K. Kimura, Transplantation of human dental pulp stem cells ameliorates brain damage following acute cerebral ischemia. ***Biomedicine & Pharmacotherapy*** 108, 1005–1014 (2018).

S. Gronthos, M. Mankani, J. Brahim, P. G. Robey, and S. Shi, Postnatal human dental pulp stem cells (DPSCs) in vitro and in vivo. ***Proceedings of the National Academy of Sciences of the United States of America*** 97, 13625–13630 (2000).

Y. Yamamoto, S. Nomura, A. Hosoi, K. Nagaoka, T. Iino, T. Yasuda, T. Saito, H. Matsushita, E. Uchida, Y. Seto, J. R. Goldenring, K. Kakimi, M. Tatematsu, and T. Tsukamoto, Established gastric cancer cell lines transplantable into C57BL/6 mice show fibroblast growth factor receptor 4 promotion of tumor growth. ***Cancer Science*** 109(5), 1480–1492 (2018).

K. Nagaoka, H. Nakanishi, H. Tanaka, J. Anindita, T. Kawamura, T. Tanaka, T. Yamashita, A. Kuroda, S. Nomura, H. Akita, K. Itaka, T. Kodama, and K. Kakimi, Neoantigen mRNA vaccines induce progenitor-exhausted T cells that support anti-PD-1 therapy in gastric cancer with peritoneal metastasis. ***Gastric Cancer*** 28(5), 825–836 (2025).

E. Darrouzet, S. Lindenthal, D. Marcellin, J.-L. Pellequer, and T. Pourcher, The sodium/iodide symporter: state of the art of its molecular characterization. ***Biochimica et Biophysica Acta*** 1838(1 Pt B), 244–253 (2014).

T. Watabe, Y. Liu, K. Kaneda-Nakashima, T. Sato, Y. Shirakami, K. Ooe, A. Toyoshima, E. Shimosegawa, Y. Wang, H. Haba, T. Nakano, A. Shinohara, and J. Hatazawa, Comparison of the therapeutic effects of [211At]NaAt and [131I]NaI in an NIS-expressing thyroid cancer mouse model. ***International Journal of Molecular Sciences*** 23(16), 9434 (2022).

S. Yamamoto, M. Yoshino, K. Kamada, R. Yajima, A. Yoshikawa, K. Nakanishi, and J. Kataoka, Development of an ultrahigh-resolution real-time alpha-particle imaging system for observing the trajectories of alpha particles in a scintillator. ***Scientific Reports*** 13(1), 4955 (2023).

M. Yoshino, A. Sugiyama, T. Tatsumi, S. Nomura, S. Shimazoe, S. Yamamoto, A. Taguchi, T. Tanaka, M. Kobayashi, and Y. Wada, Observation of At-211 accumulated cells using a real-time alpha-particle imaging system. ***RIKEN Accelerator Progress Report***, accepted (2025).

L. Jiang, Y.-Q. Zhu, R. Du, Y.-X. Gu, L. Xia, F. Qin, and H. H. Ritchie, The expression and role of stromal cell–derived factor-1α–CXCR4 axis in human dental pulp. ***Journal of Endodontics*** 34(8), 939–944 (2008).

S. Yamaguchi, R. Shibata, N. Yamamoto, M. Nishikawa, H. Hibi, T. Tanigawa, M. Ueda, T. Murohara, and A. Yamamoto, Dental pulp–derived stem cell conditioned medium reduces cardiac injury following ischemia–reperfusion. ***Scientific Reports*** 5, 16295 (2015).

M. Li, X. Sun, L. Ma, L. Jin, W. Zhang, M. Xiao, and Q. Yu, SDF-1/CXCR4 axis induces human

594 dental pulp stem cell migration through FAK/PI3K/Akt and GSK3β/β-catenin pathways.
595 ***Scientific Reports*** 7, 40161 (2017).
596
597 V. C. M. Neves, V. Yianni, and P. T. Sharpe, Macrophage modulation of dental pulp stem cell
598 activity during tertiary dentinogenesis. ***Scientific Reports*** 10(1), 20216 (2020).
599
600 C. Kornsuthisopon, A. Chansaenroj, J. Manokawinchoke, K. A. Tompkins, N. Pirarat, and T.
601 Osathanon, Non-canonical Wnt signaling participates in Jagged1-induced osteo/odontogenic
602 differentiation in human dental pulp stem cells. ***Scientific Reports*** 12(1), 7583 (2022).
603
604 M. Irfan and S. Chung, C5L2 modulates BDNF production in human dental pulp stem cells via
605 the p38α pathway. ***Scientific Reports*** 13(1), 74 (2023).
606
607 R. Antoon, N. Overdevest, A. H. Saleh, A. Keating. Mesenchymal stromal cells as cancer
608 promoters. ***Oncogene*** 43, 3545–3555 (2024). doi:10.1038/s41388-024-03183-1.
609
610 C. Stoicov, H. Li, J. H. Liu, J. Houghton. Mesenchymal stem cells utilize CXCR4–SDF-1
611 signaling for acute, but not chronic, trafficking to gastric mucosal inflammation. ***Dig. Dis. Sci.***

58, 2466–2477 (2013). doi:10.1007/s10620-013-2782-y.

F. Xiao, H. Li, Z. Feng, L. Huang, L. Kong, M. Li, D. Wang, F. Liu, Z. Zhu, Y. Wei, W. Zhang. Intermedin facilitates hepatocellular carcinoma cell survival and invasion via ERK1/2–EGR1/DDIT3 signaling cascade. ***Sci. Rep.*** 11, 488 (2021). doi:10.1038/s41598-020-80066-x.

S. Suda, C. Nito, M. Ihara, Y. Iguchi, T. Urabe, Y. Matsumaru, N. Sakai, and K. Kimura; J-REPAIR Trial Group, Randomised placebo-controlled multicentre trial to evaluate the efficacy and safety of JTR-161, allogeneic human dental pulp stem cells, in patients with acute ischaemic stroke (J-REPAIR). ***BMJ Open*** 12(5), e054269 (2022).

X. Yin, N. Sato, A. Nambu, Y. Shigekawa, and H. Haba, Progress of 211At production at the RIKEN AVF cyclotron. ***RIKEN Accelerator Progress Report*** 56, 151 (2023).

X. Yin, N. Sato, A. Nambu, Y. Kanayama, Y. Shigekawa, and H. Haba, Modification of 211At production apparatus to increase its production efficiency. ***RIKEN Accelerator Progress Report*** 57, 149 (2024).

T. Watabe, K. Mukai, S. Naka, H. Sasaki, T. Kamiya, T. Hayakawa, A. Fukuhara, T. Takano, Y. Shirakami, K. Ooe, S. Shigeno, S. Okamura, K. Masumura, E. Hida, H. Haba, A. Toyoshima, K. Isohashi, I. Shimomura, N. Tomiyama. First-in-human study of [211At]NaAt as targeted α-therapy in patients with radioiodine-refractory thyroid cancer (Alpha-T1 trial). ***J. Nucl. Med.*** Published online 25 September 2025.

M. Kanda, Y. Kasahara, D. Shimizu, T. Miwa, S. Umeda, K. Sawaki, S. Nakamura, Y. Kodera, S. Obika. Amido-bridged nucleic acid–modified antisense oligonucleotides targeting SYT13 to treat peritoneal metastasis of gastric cancer. ***Mol. Ther. Nucleic Acids*** 22, 791–802 (2020).

642 **FIGURE LEGENDS**

643 **Figure 1. Isolation and characterization of dental pulp cells (DPCs).**

644 (a) The dental pulp is a soft connective tissue located within the interior of the tooth.

645 (b) After extraction of the dental pulp tissue, the connective components were enzymatically

646 digested, mechanically minced with a sharp blade, and cultured in growth medium. Proliferating

647 cells were isolated and purified as DPCs.

648 (c) Colony-forming assay of DPCs. HeLa cells were used as a control. Cells were cultured for 0

649 or 7 days, then stained with a fluorescent dye. Fluorescence intensity was quantified as relative

650 fluorescence units (RFU; n = 3). Representative microscopic images of colonies are shown. Scale

651 bar, 200 μm.

652

653 **Figure 2. Confirmation of DPC accumulation in peritoneal tumor tissue.**

654 (a–c) Histological observation of peritoneal tumor tissue 1.5 weeks after intraperitoneal

655 administration of DPCs. Nuclei were counterstained with hematoxylin and eosin stain, and DPCs

656 were detected by immunostaining using an anti-human Lamin B1 antibody followed by an HRP-

657 conjugated secondary antibody. Panel (a) shows a low-magnification image, and (b) shows a high-

658 magnification view of the region. Arrows indicate DPCs accumulated within peritoneal tumor

659 lesions. Panel (c) shows tissue from a normal mouse injected with DPCs as a control. (scale

660 bars=50 μm in a&c, scale bar=100 μm in b.)

661 (d) Migration assay evaluating DPC chemotaxis toward YTN16 gastric cancer cells. The lower

662 chamber contained 5×10^4 to 2×10^5 YTN16 cells, and 1×10^5 DPCs were seeded in the upper

663 chamber. After 48 hours, calcein staining was performed and fluorescence intensity of migrated

664 cells was quantified. DPC migration increased in proportion to the number of YTN16 cells in the

665 lower chamber ($n = 4$; $^{**}p < 0.01$).

666

667 **Figure 3. Functional transduction of the sodium/iodide symporter (NIS) into DPCs.**

668 (a) Gene expression levels of parental DPCs and sodium/iodide symporter (NIS)–transduced

669 DPCs (NIS-DPCs) quantified from RNA-seq data and presented as transcripts per million (TPM)

670 values. Among iodide symporter genes, SLC5A5 was transduced and expressed in NIS-DPC.

671 GAPDH and beta-actin (ACTB) were controls (n=3).

672 (b) Correlation analysis between NIS-positive cell fraction and iodide uptake levels in NIS-DPCs.

673 (c) Comparison of iodide uptake between DPCs and NIS-DPCs. Data for NIS-DPCs were

674 obtained from different lots.

675 (d–g) Macroscopic and fluorescence imaging analyses of a gastric cancer peritoneal

676 dissemination model after intraperitoneal administration of DiR-labeled DPCs. Panels (d) and (e)

677 show macroscopic views of the peritoneal serosa, where blue lines outline the regions of

678 peritoneal tumor nodules. Corresponding in vivo imaging system (IVIS) fluorescence images (f

679 and g) demonstrate colocalization of fluorescence signals with the tumor lesions identified in (d)

680 and (e).

681 (h~j) *In vivo* localization of NIS-DPCs within tumor tissue, showing accumulation comparable to

682 that of unmodified DPCs. Scale bars=50 μm in h&j, scale bar=100 μm in i.

683 (k) Migration assay using Transwell chambers with YTN16 gastric cancer cells placed in the

684 lower compartment. NIS-DPCs exhibited cell number–dependent migration similar to DPCs (n =

685 3; **$p < 0.01$).

686

687 **Figure 4. Preparation and functional characterization of sodium astatide-211 (Na[At-211])**

688 **and its uptake by NIS-DPCs.**

689 (a) Reaction protocol for converting purified free At-211, produced at an accelerator facility, into

690 a homogeneous sodium astatide form (Na[At-211]). The free isotope can exist in multiple

691 chemical species, and sodium conjugation was performed to stabilize its form.

692 (b) Thin-layer chromatography (TLC) analysis of At-211 before and after sodium conjugation.

693 Left: TLC profile of free At-211 (~100 kBq). Right: TLC profile of Na[At-211] (~280 kBq).

694 Arrows indicate the Na[At-211] peak position.

695 (c) Cellular uptake of Na[At-211] by DPCs and NIS-DPCs. DPCs or NIS-DPCs (5×10^4 cells per

696 well) were seeded in 24-well plates and incubated with 10 kBq Na[At-211]. At 5, 10, and 60 min,

697 cells were collected, fractionated, and measured for protein concentration and radioactivity.

698 Radioactivity normalized to protein content was calculated. NIS-DPCs exhibited approximately

699 tenfold higher At-211 uptake than parental DPCs (n = 3; black bars, DPCs; gray bars, NIS-DPCs).

700

701 **Figure 5. Detection of alpha-particle emission from NIS-DPCs.**

702 (a) Schematic diagram of the alpha-particle detection system. alpha-particles emitted from cells

703 (left) are first converted into photons by a GAGG:Ce scintillator. The photons are then amplified

704 and reflected within the detector and captured by a cooled CMOS sensor positioned at the top.

705 (b) Overview of the alpha-particle detection device.

706 (c–e) NIS-DPCs (1.8×10^4 cells per well) were seeded in 8-well chamber slides and incubated

707 for 30 min with 500 kBq of Na[At-211]. Cells were then fixed with formalin and imaged.

708 Arrowheads indicate the localization of individual cells.

709 (f–h) DPCs (1.8×10^4 cells per well) were similarly treated with 500 kBq Na[At-211], incubated

710 for 30 min, fixed with formalin, and imaged.

711 (c and f) Optical microscopic images of cells. (d and g) Corresponding alpha-camera signal

712 images. (e and h) Merged images combining optical and alpha-particle signals. Scale bar=100 μm.

713

714 **Figure 6. Therapeutic efficacy of NIS-DPCs combined with At-211 in a murine gastric**

715 **cancer peritoneal dissemination model.**

716 To establish a peritoneal dissemination model, C57BL/6 mice were inoculated

717 intraperitoneally with 1×10^7 YTN16 gastric cancer cells. Two days prior to nucleotide injection,

718 0.5×10^6 NIS-DPCs were administered intraperitoneally. Then, two weeks after YTN16

719 transplantation, 0.6 MBq of Na[At-211] was injected intraperitoneally. The mice were sacrificed

720 1.5 weeks later for macroscopic observation.

721 (a) Untreated control mouse.

722 (b) A mouse that received an intraperitoneal injection of NIS-DPCs only.

723 (c) A mouse that was treated with DPCs and Na[At-211].

724 (d) A mouse that received an intraperitoneal administration of NIS-DPCs, followed by Na[At-

725 211]. The peritoneal tumor burden disappeared after treatment with NIS-DPCs and Na[At-211].

726 Asterisks indicate a smooth peritoneum.

727 (e) Macroscopic scoring of peritoneal dissemination was performed on a 0–4 scale.

728 (f) Quantitative comparison of macroscopic scores among the untreated group, Na[At-211]-only

729 group, and the group receiving three NIS-DPC administrations plus Na[At-211]. Statistical

730 analysis was performed using Tukey's test ($n = 10$; $^{**}p < 0.01$, $^{***}p < 0.001$).

731 (g) Kaplan–Meier survival analysis after one month following Na[At-211] administration. Mice

treated with three administrations of NIS-DPCs plus Na[At-211] (#3) showed a significant survival advantage compared with the untreated group (#1) and the Na[At-211]-only group (#2). Control groups without YTN16 cell implantation included Na[At-211]-only (#4) and NIS-DPC × 3 + Na[At-211] (#5) treatments (#1 : n = 16, #2/3 : n = 17, #4/5 : n = 3; *p < 0.05, **p < 0.01).

Figure 7. Graphical Summary. Stepwise overview of the NIS-DPC cancer-targeting concept. The schematic illustrates the translational workflow of NIS-DPCs as a targeted theranostic platform for cancer therapy.

Step 1 (engineering). DPCs were genetically modified to express the sodium/iodide symporter (NIS), which mediates the cellular uptake of both iodide and astatine. The lower panel depicts this dual transport function of NIS, highlighting its ability to internalize iodide and the αalpha-emitting radionuclide At-211.

Step 2 (targeting and accumulation). Following administration, NIS-DPCs preferentially accumulated in cancer cells, enabling the selective delivery of At-211 to tumor sites.

Step 3 (localized therapy/outcome). Localized α radiation at the tumor site induced targeted cytotoxicity, demonstrating the translational potential of NIS-DPC–mediated therapy for precise cancer treatment.

Fig.1a&b

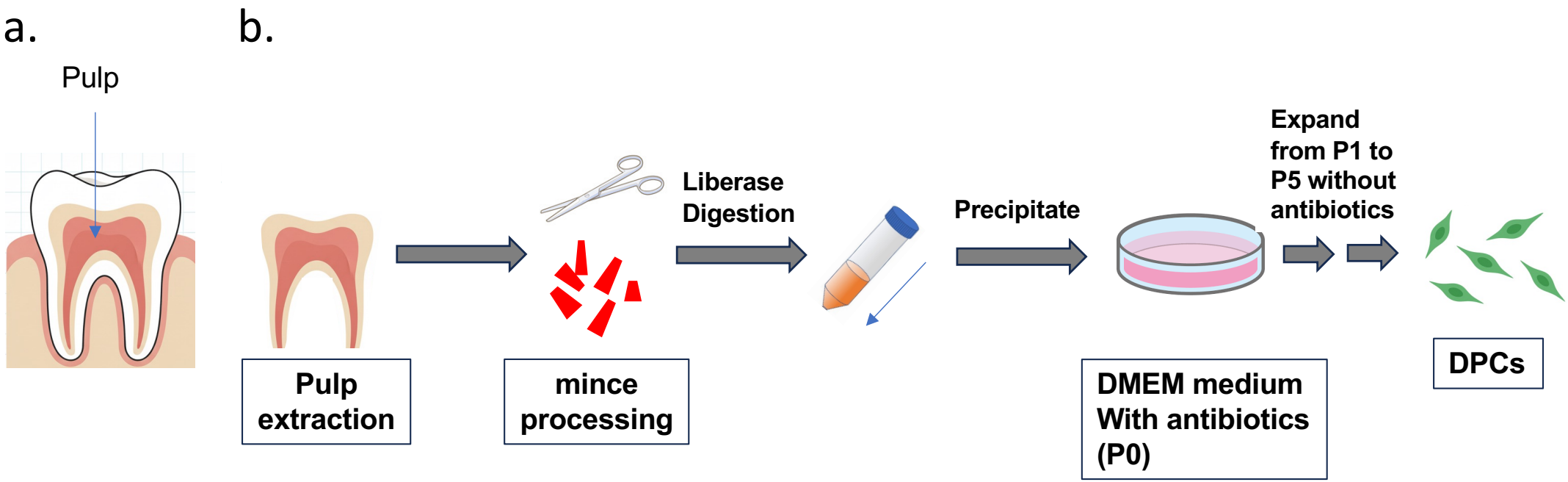
a.
Pulp
b.
Pulp extraction
mince processing
Liberase Digestion
Precipitate
DMEM medium With antibiotics (P0)
Expand from P1 to P5 without antibiotics
DPCs

Fig.1c

c.

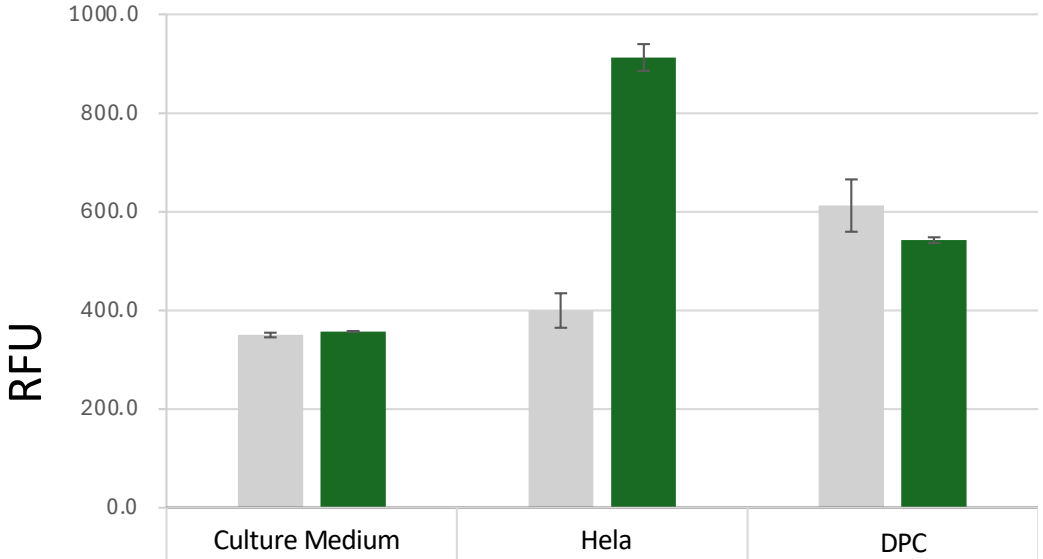

	Culture Medium	Hela	DPC
Day0	350.1	399.7	612.4
Day7	357.2	912.5	542.3

【Day0】

【Day7】

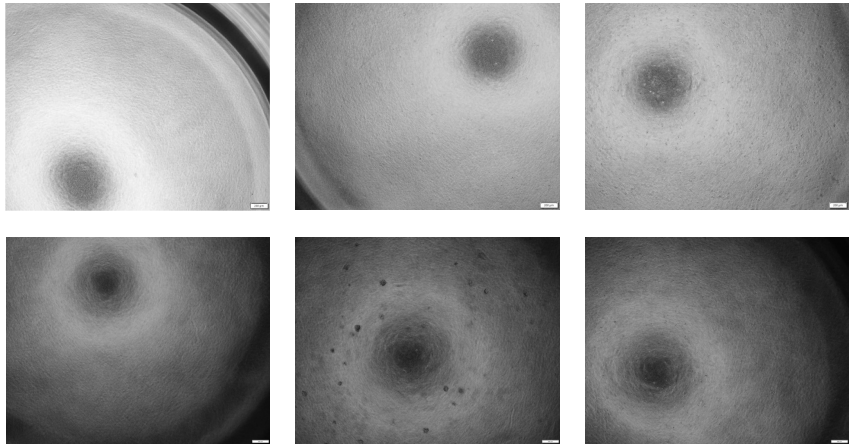

Fig. 2a~c

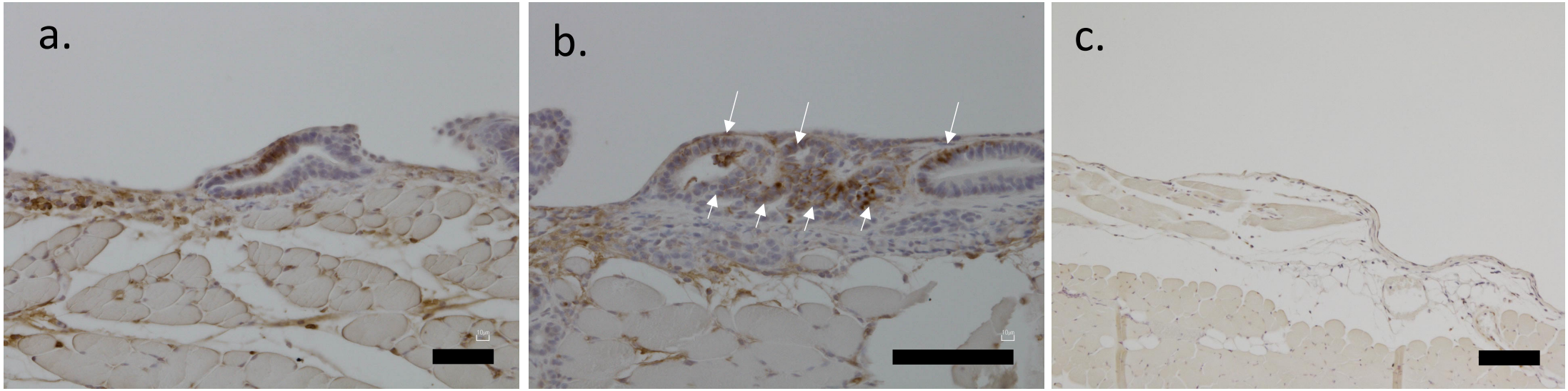

Fig. 2d

d.

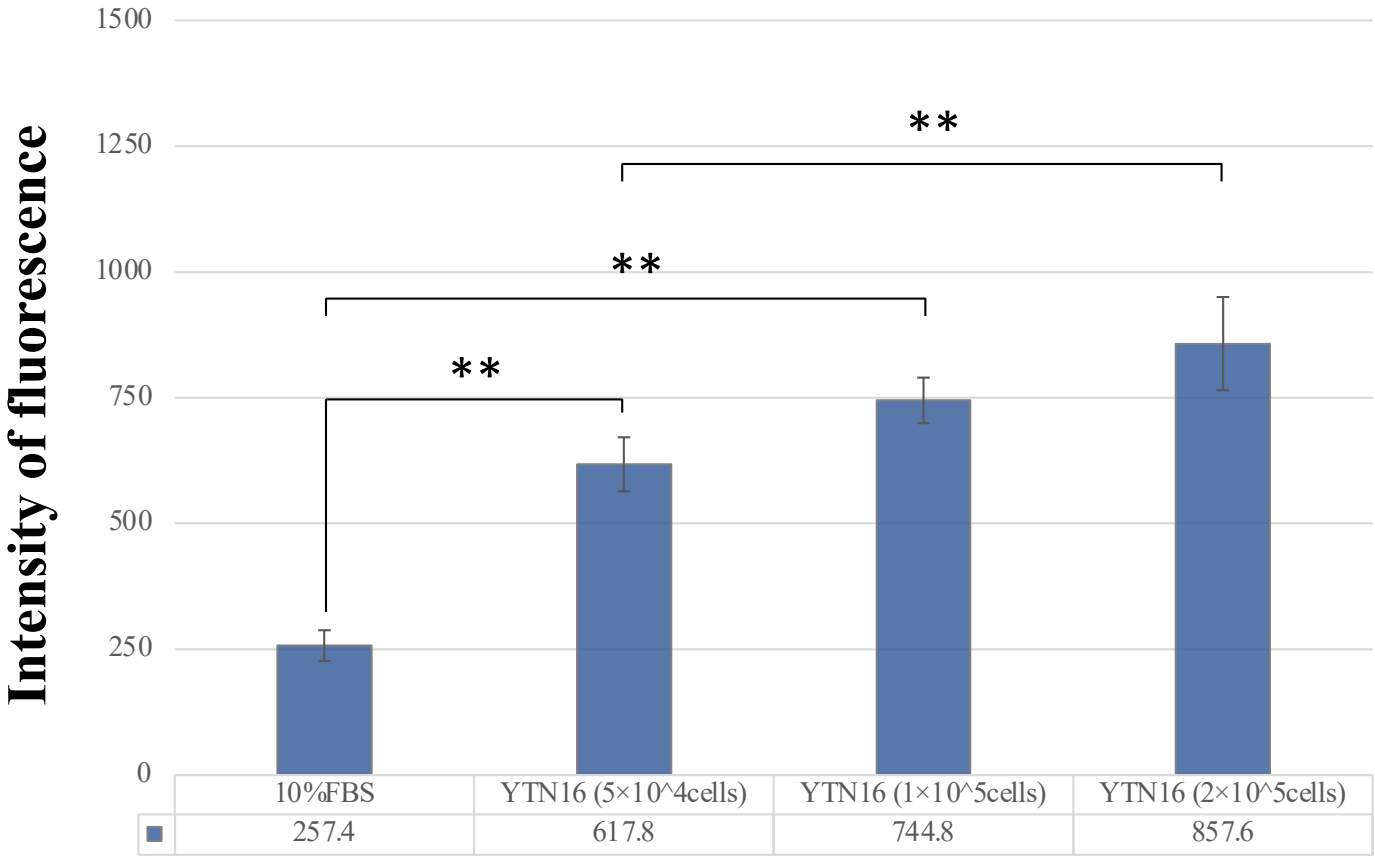
Intensity of fluorescence
1500
1250
1000
750
500
250
0
**
**
**
10%FBS
YTN16 (5×10^4cells)
YTN16 (1×10^5cells)
YTN16 (2×10^5cells)
257.4
617.8
744.8
857.6

Fig. 3a

a.

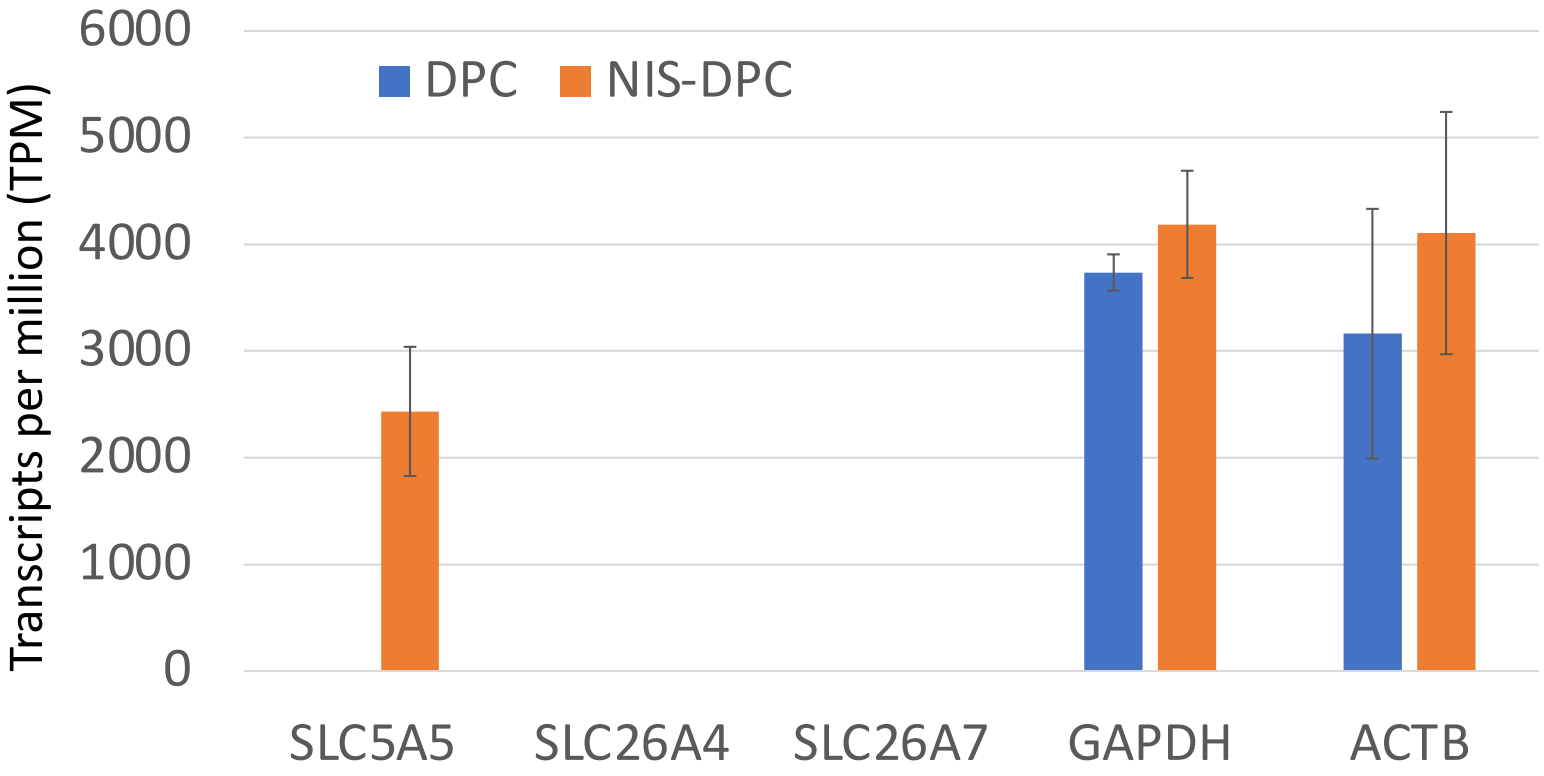
6000
5000
4000
3000
2000
1000
0
Transcripts per million (TPM)
DPC
NIS-DPC
SLC5A5
SLC26A4
SLC26A7
GAPDH
ACTB

Fig.3 b&c

b.

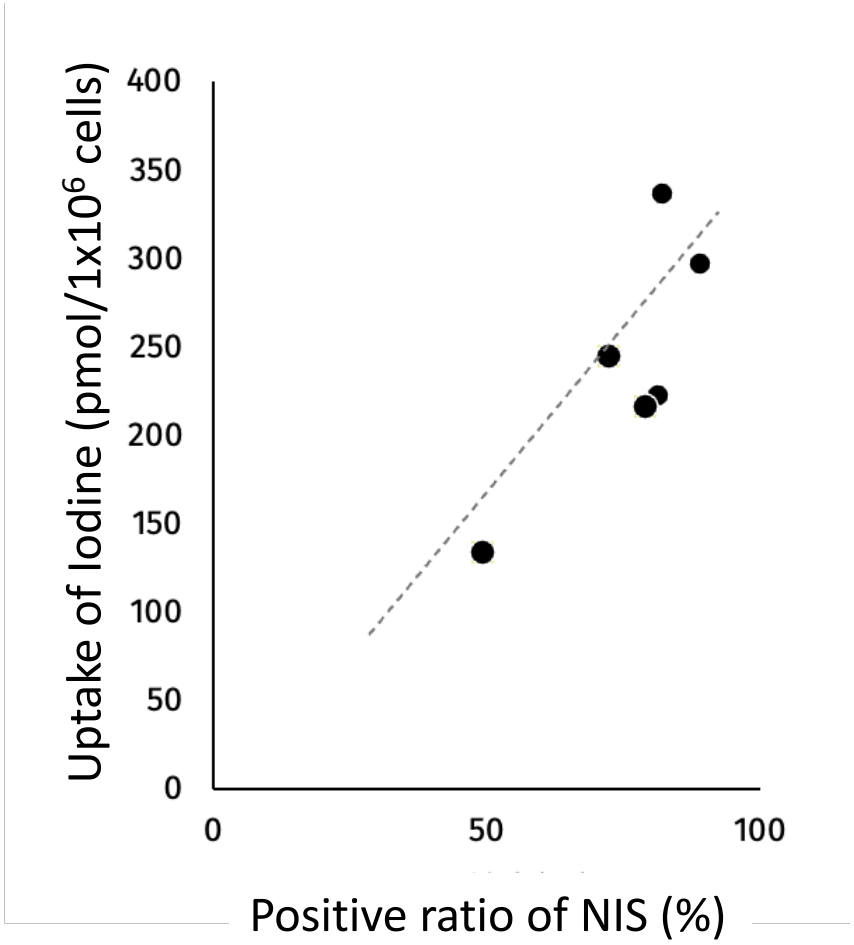
Uptake of Iodine (pmol/1x10^6 cells)
400
350
300
250
200
150
100
50
0
0
50
100
Positive ratio of NIS (%)

c.

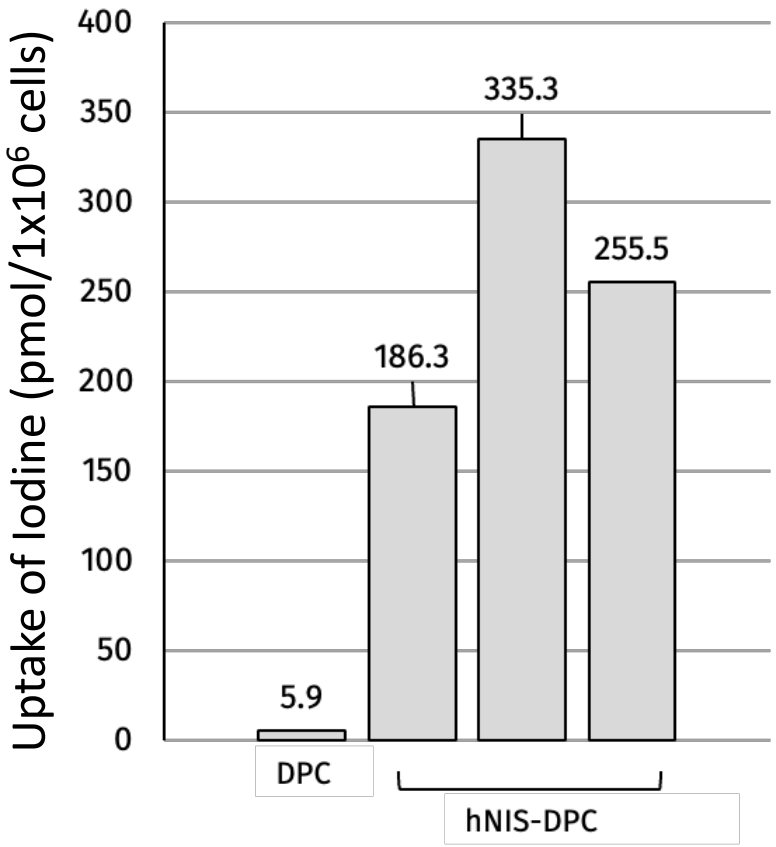
Uptake of Iodine (pmol/1x10^6 cells)
400
350
300
250
200
150
100
50
0
5.9
186.3
335.3
255.5
DPC
hNIS-DPC

Fig.3 d~g

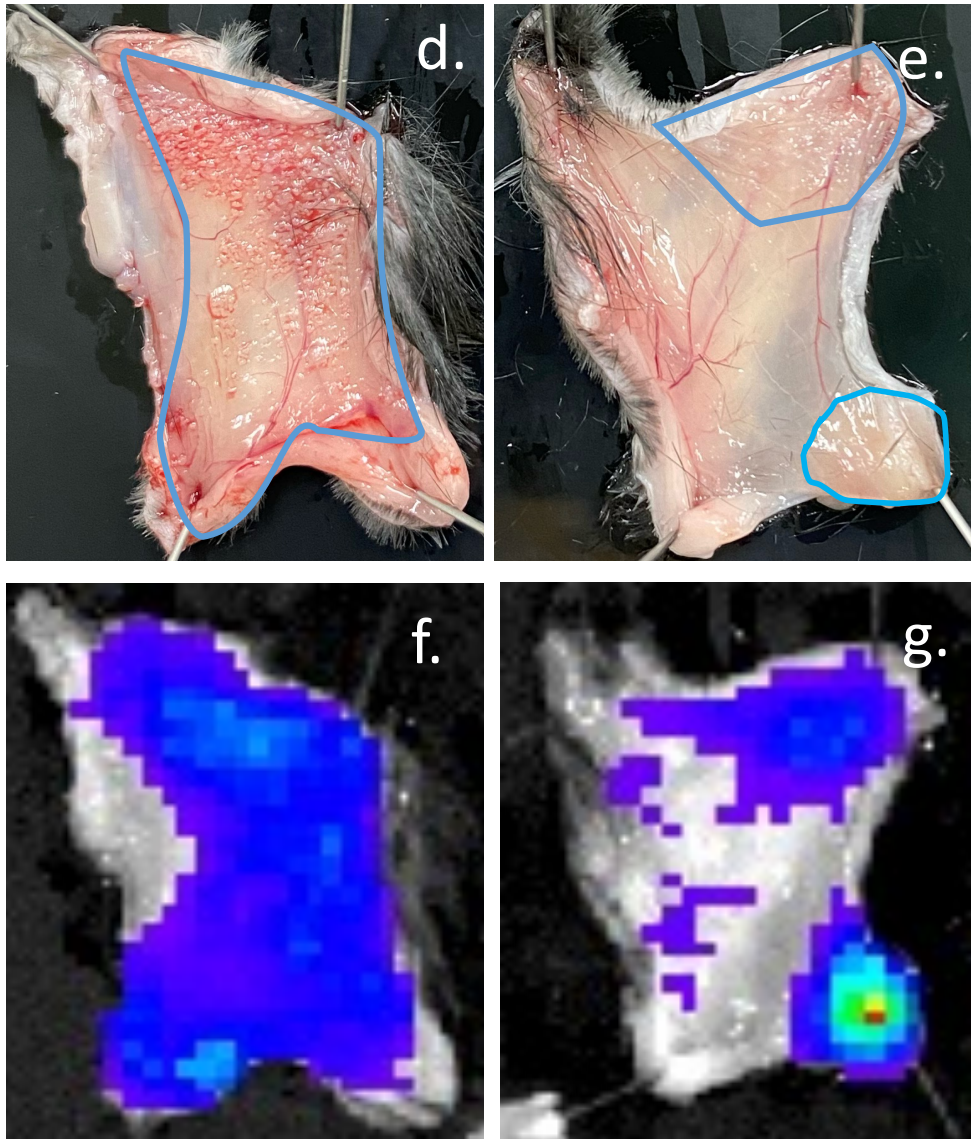

Fig.3 h~j

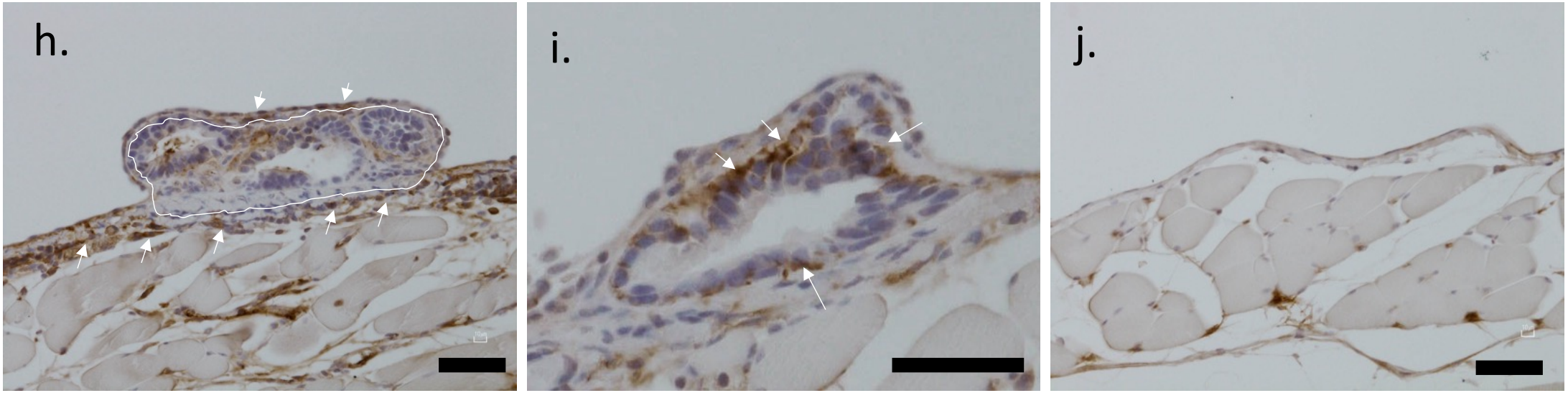

Fig.3 k

k.

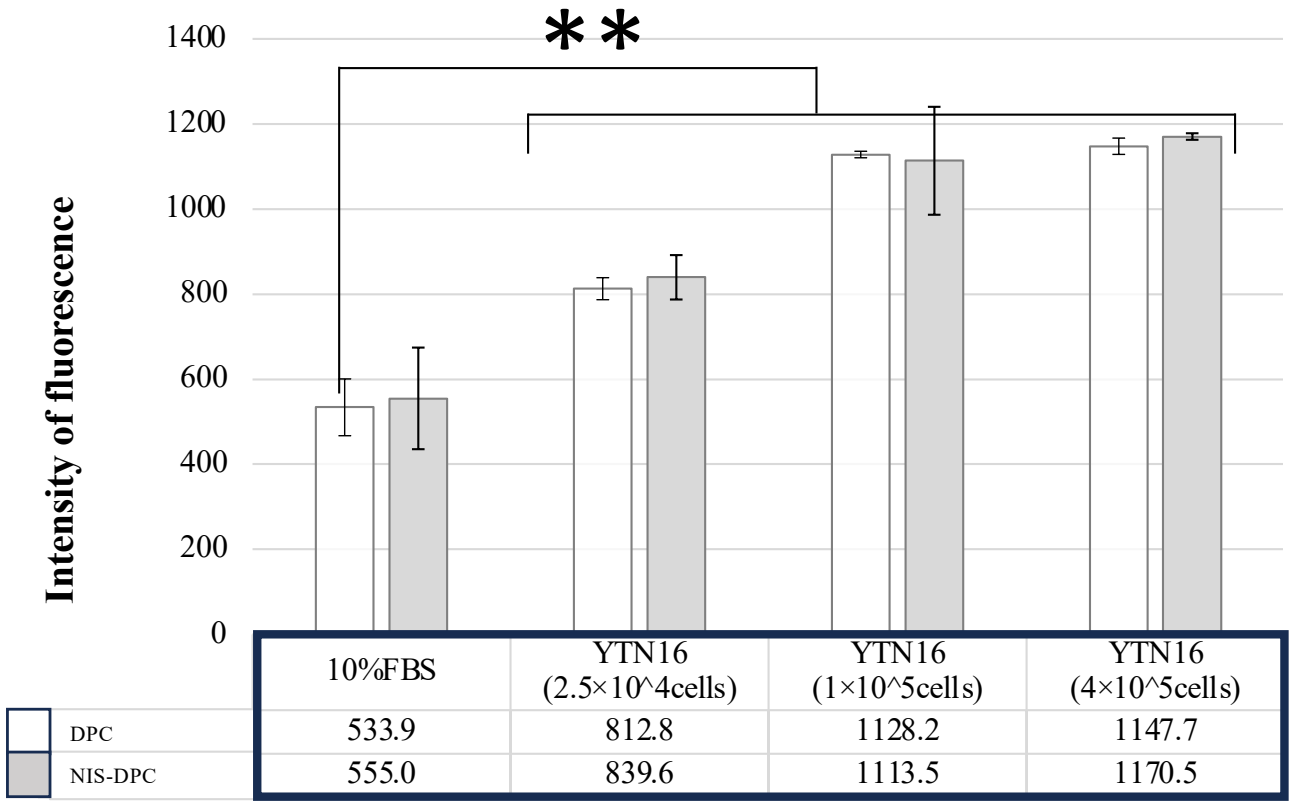
**
1400
1200
1000
800
600
400
200
0
Intensity of fluorescence
10%FBS
YTN16 (2.5×10^4cells)
YTN16 (1×10^5cells)
YTN16 (4×10^5cells)
DPC
NIS-DPC
533.9
812.8
1128.2
1147.7
555.0
839.6
1113.5
1170.5

Fig. 4a&b

a.

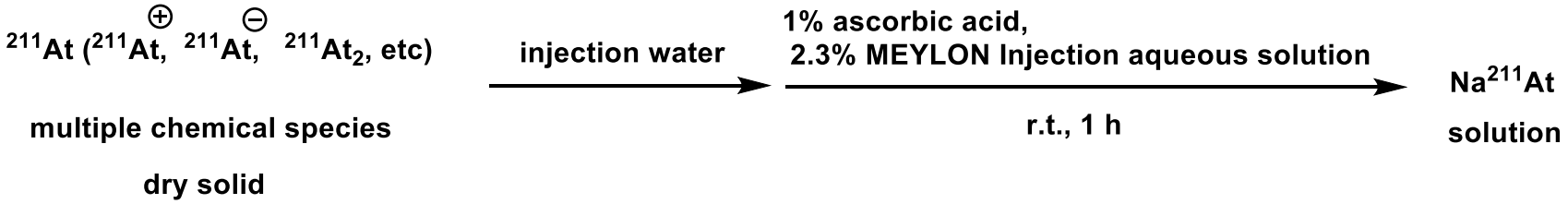
^{211}At ($^{211}At^{\oplus}$, $^{211}At^{\ominus}$, $^{211}At_2$, etc)
multiple chemical species
dry solid
injection water
1% ascorbic acid,
2.3% MEYLON Injection aqueous solution
r.t., 1 h
$Na^{211}At$
solution

b.

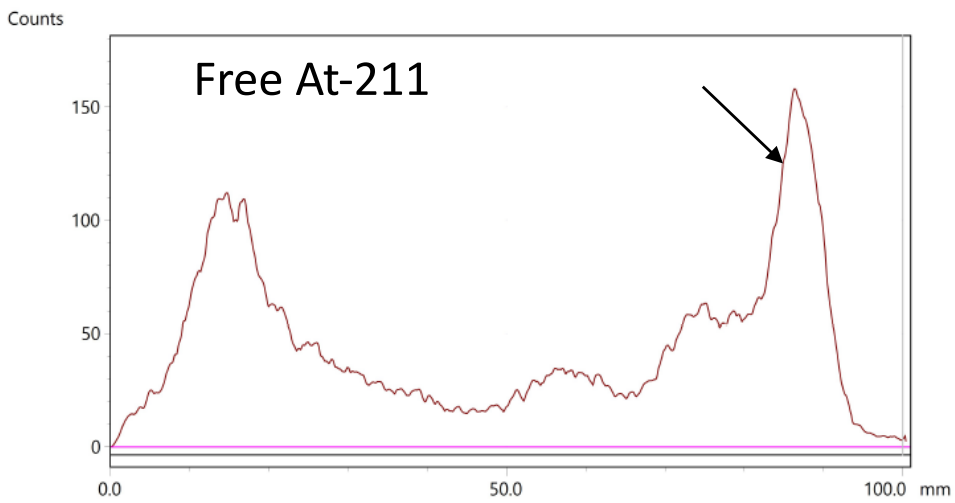
Counts
Free At-211
150
100
50
0
0.0
50.0
100.0 mm

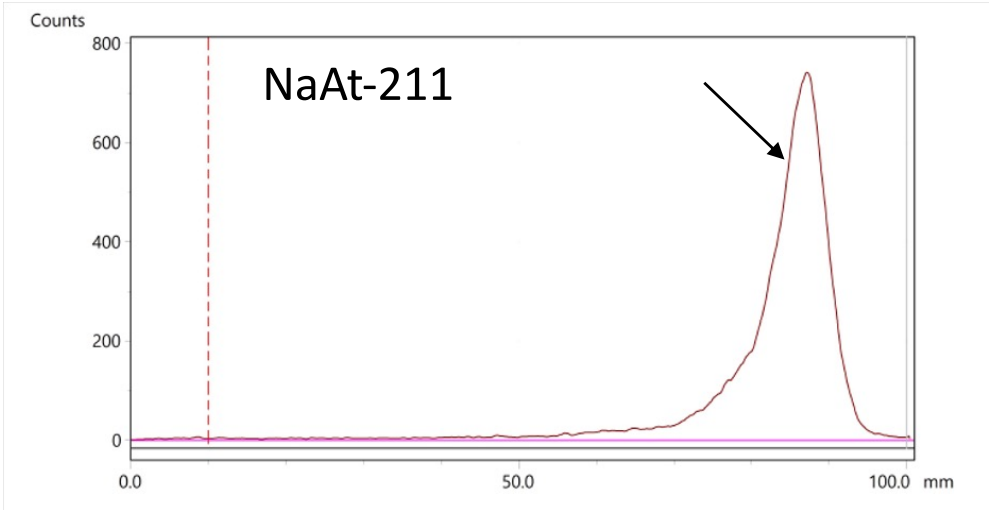
Counts
NaAt-211
800
600
400
200
0
0.0
50.0
100.0 mm

Fig. 4c

c.

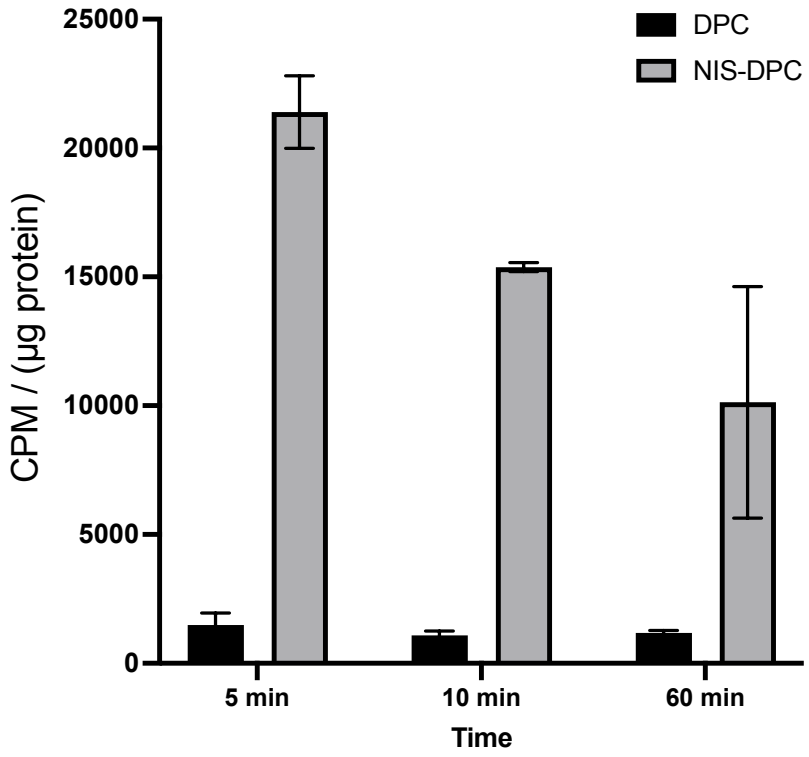
DPC
NIS-DPC
25000
20000
15000
10000
5000
0
CPM / (µg protein)
5 min
10 min
60 min
Time

Fig. 5

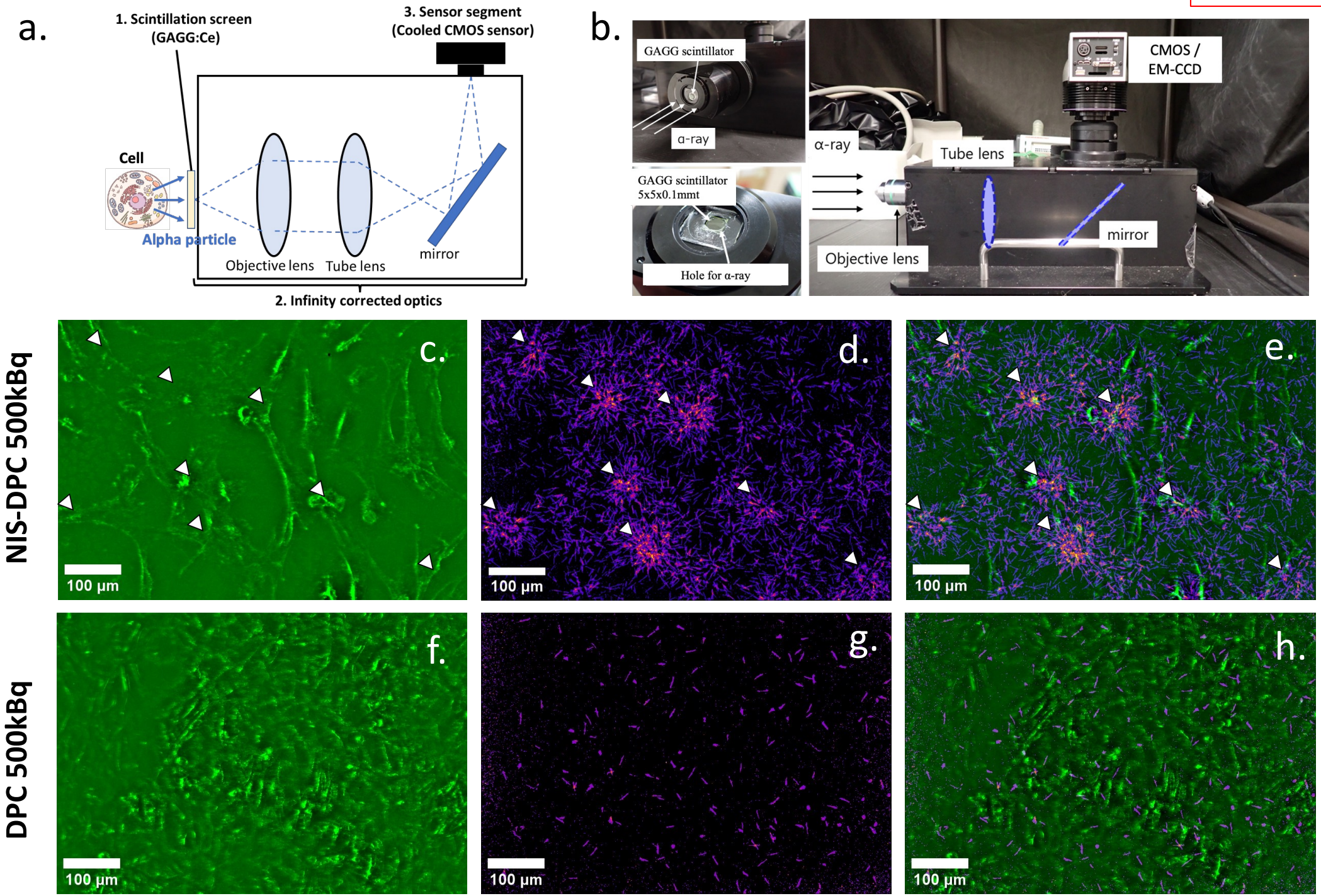
a.
1. Scintillation screen
(GAGG:Ce)
3. Sensor segment
(Cooled CMOS sensor)
Cell
Alpha particle
Objective lens
Tube lens
mirror
2. Infinity corrected optics
b.
GAGG scintillator
α-ray
GAGG scintillator
5x5x0.1mmt
Hole for α-ray
CMOS /
EM-CCD
α-ray
Tube lens
mirror
Objective lens
NIS-DPC 500kBq
DPC 500kBq
c.
d.
e.
f.
g.
h.
100 μm

Fig.6a~d

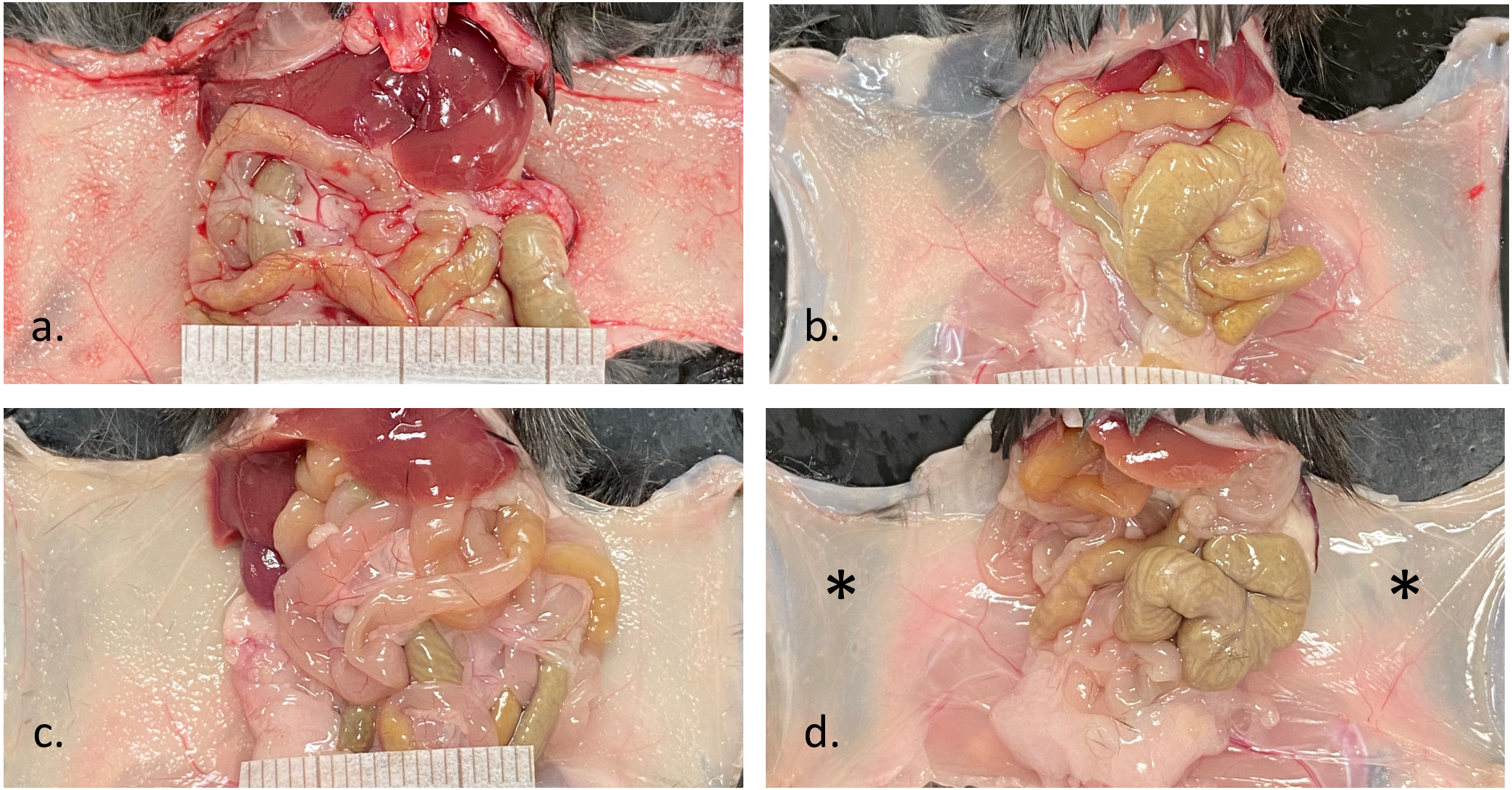

Fig.6 e&f

e.

Macroscopic Score Evaluation of Peritoneal Tissue by Gross Examination
Rating scale: 0 (lowest) to 4 (highest)

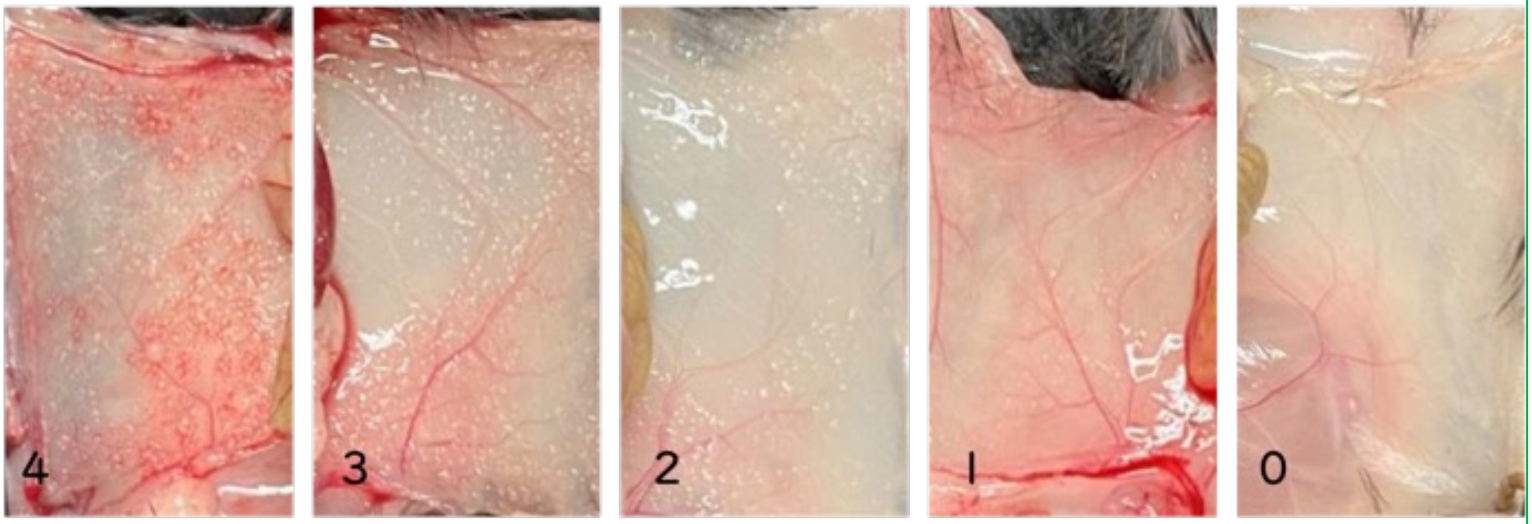

4	3	2	1	0
The grains are large and uniform throughout.	There are some grains, but not all over.	Clearly present, but the grains are small and watery.	Upon closer inspection, it exists only faintly.	No tumor

f.

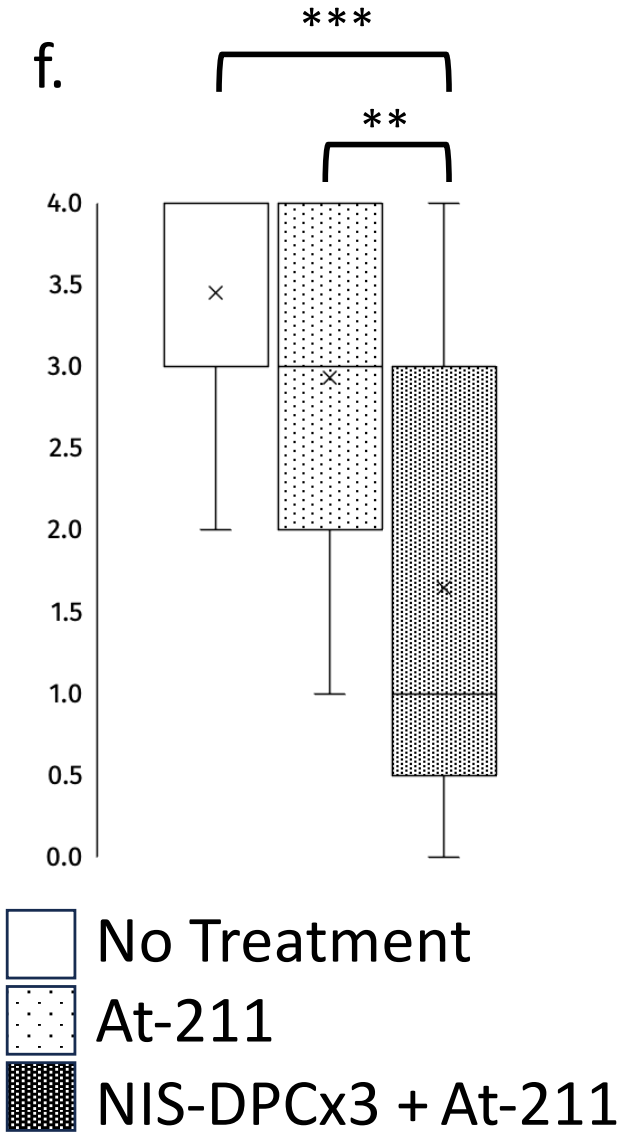

Fig.6g

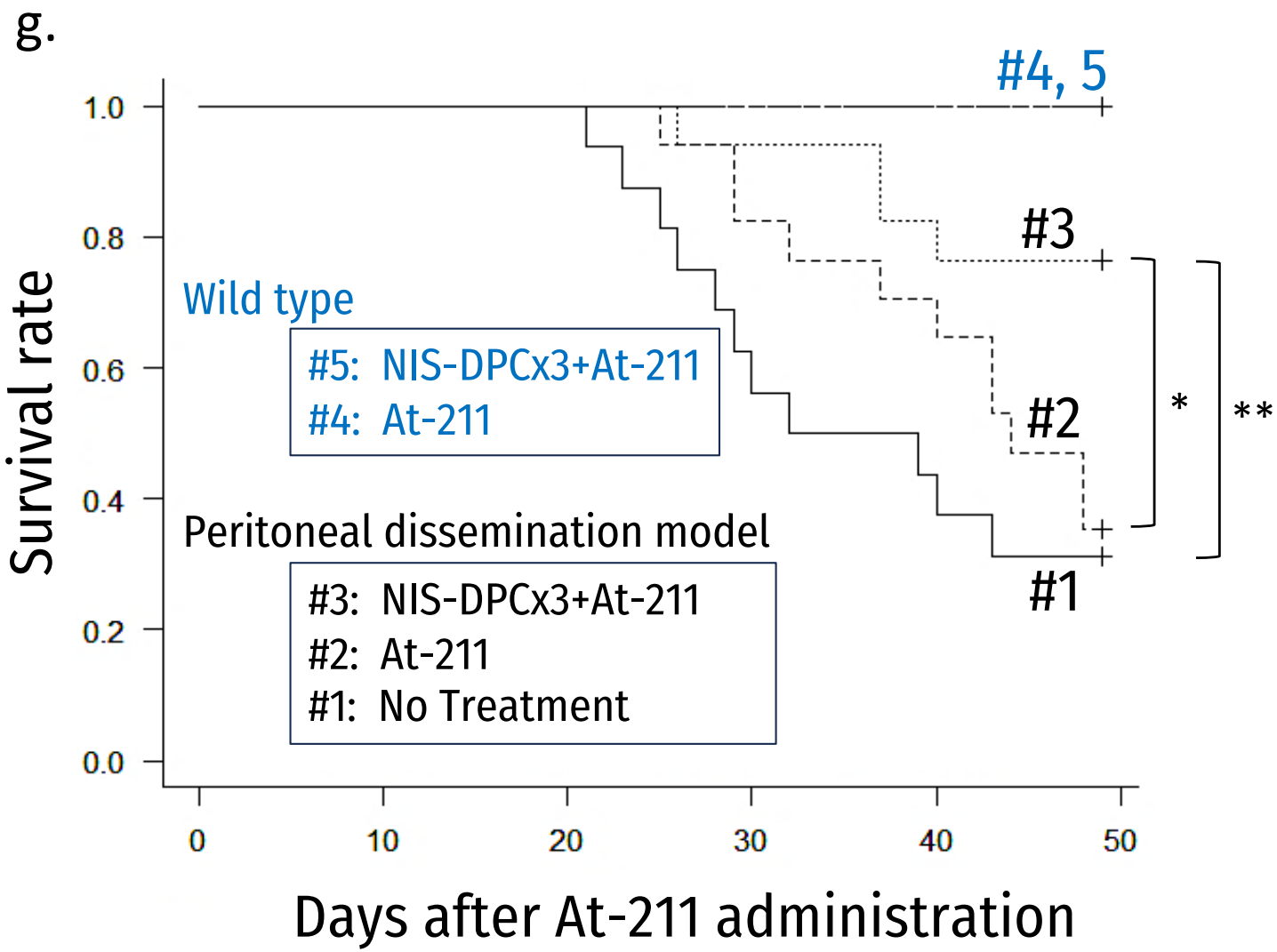
g.
Survival rate
1.0
0.8
0.6
0.4
0.2
0.0
0
10
20
30
40
50
Days after At-211 administration
#4, 5
#3
#2
#1
*
**
Wild type
#5: NIS-DPCx3+At-211
#4: At-211
Peritoneal dissemination model
#3: NIS-DPCx3+At-211
#2: At-211
#1: No Treatment

Fig. 7

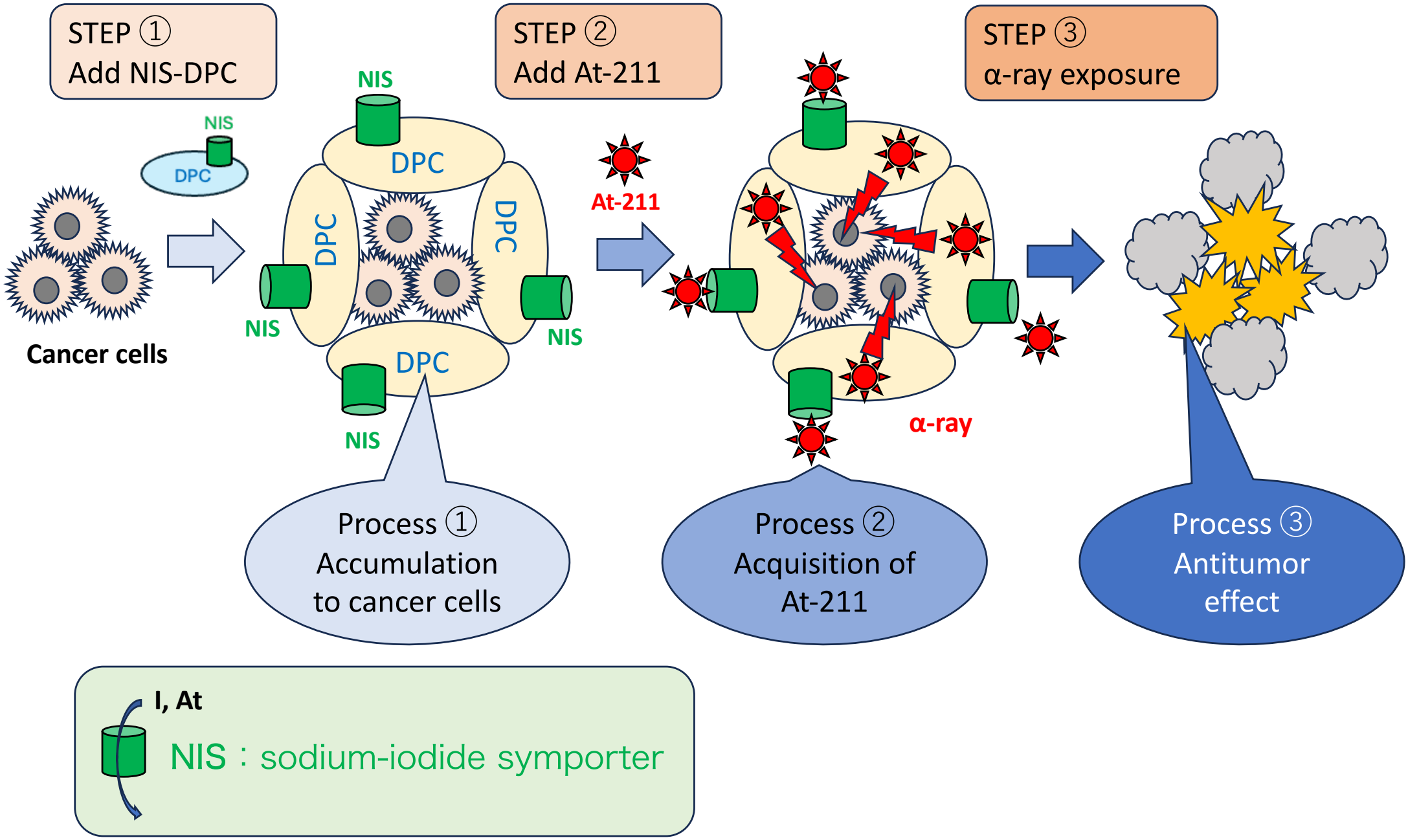
STEP ①
Add NIS-DPC
STEP ②
Add At-211
STEP ③
α-ray exposure
NIS
DPC
Cancer cells
At-211
α-ray
Process ①
Accumulation
to cancer cells
Process ②
Acquisition of
At-211
Process ③
Antitumor
effect
I, At
NIS : sodium-iodide symporter